REPORT 1301

LINEARIZED LIFTING-SURFACE AND LIFTING-LINE EVALUATIONS OF SIDEWASH BEHIND ROLLING TRIANGULAR WINGS AT SUPERSONIC SPEEDS [1]

By Percy J. Bobbitt

SUMMARY

The lifting-surface sidewash behind rolling triangular wings has been derived for a range of supersonic Mach numbers for which the wing leading edges remain swept behind the Mach cone emanating from the wing apex. Variations of the sidewash with longitudinal distance in the vertical plane of symmetry are presented in graphical form.

An approximate expression for the sidewash has been developed by means of an approach using a horseshoe-vortex approximate-lifting-line theory. By use of this approximate expression, sidewash may be computed for wings of arbitrary plan form and span loading. A comparison of the sidewash computed by lifting-surface and lifting-line expressions for the triangular wing showed good agreement except in the vicinity of the trailing edge when the leading edge approached the sonic condition.

An illustrative calculation has been made of the force induced by the wing sidewash on a vertical tail located in various longitudinal positions.

INTRODUCTION

In order to make reliable estimates of the total forces and moments acting on an aircraft, accurate evaluations are required of the loadings on the individual isolated components and of the interference effects between components. Although considerable effort has been expended in recent years to supply much of this needed information for the supersonic speed range, many important problems remain. Among these is the induced effect of the wing flow field or, more precisely, the wing sidewash on the vertical tail. The only specific numerical results of this nature obtained to date have been for the angle-of-attack motion. In the vertical plane of symmetry for this case, however, the sidewash is zero and tail surfaces located in this plane are unaffected. This is not the situation for the rolling, yawing, and sideslipping motions where the sidewash in the vertical plane of symmetry is finite and the load induced on the vertical tail can be appreciable. Evaluation of the sidewash for these motions would, therefore, be important in the prediction of the lateral stability of supersonic aircraft.

The present report presents the derivation of the sidewash behind steady rolling, triangular wings with subsonic leading edges. Both lifting-surface and lifting-line methods, previously applied primarily to determine downwash, are utilized and comparisons are made of the sidewash computed by the two methods in order to give an indication of the worth of the more easily obtainable lifting-line results. The lifting-surface sidewash is determined by using the doublet-distribution method of reference 1, and the lifting-line values are obtained by use of the lifting-line approach given in reference 2.

An illustrative calculation using the derived sidewash is made of the force induced on a half-delta tail operating behind a rolling triangular wing, and this force is contrasted to the force that would act on the tail if it were rolling in the undisturbed stream.

The material presented in this report was submitted to the University of Virginia as a thesis in partial fulfillment of the requirements for the degree of Master of Science in Aeronautical Engineering.

SYMBOLS

The positive directions of forces, moments, and velocities are shown in figure 1.

x, y, z	Cartesian coordinates of field point
x_1, y_1, z_1	Cartesian coordinates of doublet or line-vortex position
u, v, w	perturbation velocities along x-, y-, and z-axis, respectively
A	wing aspect ratio, b^2/S
b	wing span
C_n	yawing-moment coefficient, $\dfrac{\text{Yawing moment}}{qSb}$
$C_{n_p}=\left\lvert\dfrac{\partial C_n}{\partial \frac{pb}{2V}}\right\rvert_{p\to 0}$	
C_Y	side-force coefficient, $\dfrac{\text{Side force}}{qS}$
$C_{Y_p}=\left\lvert\dfrac{\partial C_Y}{\partial \frac{pb}{2V}}\right\rvert_{p\to 0}$	
c	wing root chord
d	distance from wing trailing edge to a point downstream
h	displacement of vortex sheet below wing trailing edge
h_1, h_2	limits of y_1-integration

[1] Supersedes NACA Technical Note 3609 by Percy J. Bobbitt, 1956.

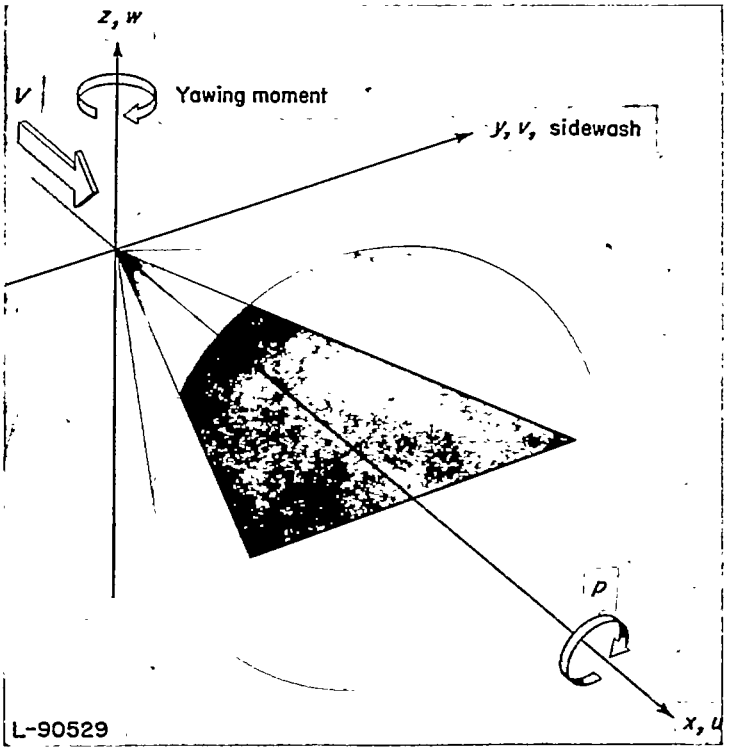

FIGURE 1.—Triangular wing oriented with respect to body system of axes used in analysis and associated symbol data.

i variable index used in summations and as subscript

k constant

$k_1=\frac{\sqrt{(x-x_1)^2-\beta^2z^2}}{\theta_0x_1}$

$k_{1,0}=\frac{\sqrt{(x-c)^2-\beta^2z^2}}{\theta_0c}$

$k_{1,0}'=\sqrt{1-k_{1,0}^2}$

$k_2=\frac{\theta_0x_1}{\sqrt{(x-x_1)^2-\beta^2z^2}}$

$k_{2,0}=\frac{\theta_0c}{\sqrt{(x-c)^2-\beta^2z^2}}$

$k_{2,0}'=\sqrt{1-k_{2,0}^2}$

M free-stream Mach number, V/Velocity of sound in free stream

m slope of lifting line

P static pressure

$\Delta P=P_l-P_u$

p angular velocity of roll, radians/sec

q free-stream dynamic pressure, $\frac{1}{2}\rho V^2$

S wing area

$\Delta u_s=u_u-u_l$

V free-stream velocity

v_P sidewash induced by doublets distributed over plan form

v_W sidewash induced by doublets distributed over wake

$X=x-x_1$

$X_t=x-x_t$

$\overline{X}_t=\frac{X_t}{b/2}$

$x_0=\frac{x}{c}$

$x_{1,0}=\frac{x_1}{c}$

$Y=y-y_1$

$Y_t=y-y_t$

$Y_{t,0}=\frac{Y_t}{b/2}$

$y_0=\frac{y}{b/2}$

$z_0=\frac{z}{b/2}$

α angle of attack, radians

$\beta=\sqrt{M^2-1}$

Γ circulation at any spanwise station

ϵ angle of downwash measured in xz-plane, between trailing vortex sheet and axis parallel to free-stream direction, radians

$\theta_0=\beta\frac{b/2}{c}\left(=\frac{\beta A}{4}\text{ for triangular wings}\right)$

λ angle through which vortex sheet rotates in moving from wing trailing edge to a point which is d distance downstream

ρ density of free-stream air

ϕ perturbation velocity potential

$\Delta\phi_s=\phi_u-\phi_l$

$a=\frac{\theta_0c}{\beta z}=\frac{1}{z_0}$

E complete elliptic integral of second kind with modulus k, $\int_0^1\frac{\sqrt{1-k^2s^2}}{\sqrt{1-s^2}}ds$

K complete elliptic integral of first kind with modulus k, $\int_0^1\frac{ds}{\sqrt{1-k^2s^2}\sqrt{1-s^2}}$

$E(t,k)$ incomplete elliptic integral of second kind with argument t and modulus k, $\int_0^t\frac{ds}{\sqrt{1-k^2s^2}\sqrt{1-s^2}}$

$F(t,k)$ incomplete elliptic integral of first kind with argument t and modulus k, $\int_0^t\frac{\sqrt{1-k^2s^2}\,ds}{\sqrt{1-s^2}}$

$f=\frac{x-\sqrt{\theta_0^2x^2+\beta^2z^2(1-\theta_0^2)}}{1-\theta_0^2}$

$f_0=\frac{x_0-\theta_0\sqrt{x_0^2+z_0^2(1-\theta_0^2)}}{1-\theta_0^2}$

$G\left(k_{2,0},\frac{1}{z_0}\right)=\frac{\pi}{2}+(K_{2,0}-E_{2,0})F\left(\cot^{-1}\frac{1}{z_0},k_{2,0}'\right)-K_{2,0}E\left(\cot^{-1}\frac{1}{z_0},k_{2,0}'\right)$

$G(\theta_0)=\frac{2-\theta_0^2}{1-\theta_0^2}E'(\theta_0)-\frac{\theta_0^2}{1-\theta_0^2}F'(\theta_0)$

$H=\frac{2p}{\beta^2 G(\theta_0)}$

L.E. leading edge

T.E. trailing edge

$\overline{\int}$ sign denoting finite part of integral

Subscripts:

D conditions in region D (fig. 2)

E conditions in region E (fig. 2)

l pertaining to lower side of surface

P plan form

s conditions on surface of discontinuity (at $z_1=0$)

u pertaining to upper side of surface

W wake

The subscripts 1,2, 1,0, and 2,0 on the elliptic functions E and K indicate the modulus of the elliptic function; that is,

$$K_1=K\left(\frac{\pi}{2}, k_1\right)$$

$$E_{2,0}=E\left(\frac{\pi}{2}, k_{2,0}\right)$$

ANALYSIS

GENERAL REMARKS

The problem to be considered herein is that of determining the perturbation sidewash velocity behind a rolling triangular wing for a range of supersonic Mach numbers for which the leading edges of the wing are subsonic. The analysis is based on an application of linearized supersonic-flow theory and, hence, the results obtained will be valid within the limitations of linear theory.

In the analysis which follows, several assumptions are made concerning the trailing vortex sheet. These assumptions are that the vortex sheet must remain flat behind the wing and that the rotation of the vortex sheet is small enough to be neglected. In addition, the nonrestrictive stipulation is made that the rolling wings be at zero angle of attack. Further discussion of these points will be found in the section entitled "Results and Discussion."

In flight, a steady rolling motion will usually be maintained by differentially deflected ailerons that create a sidewash opposed to the wing sidewash. Calculation of aileron sidewash, which may be of the same order of magnitude as the wing sidewash, will not be considered in the present report.

BOUNDARY CONDITIONS

The boundary conditions for the proposed problem may be prescribed on the $z=0$ plane and are similar to those given for the angle-of-attack motion in reference 1.

The downwash boundary condition on the rolling wing is

$$w=(py)_{p\to 0}$$

In order to analyze the quasi-steady rolling problem by use of steady-flow theory, the rolling wing is considered fixed in approximately the $z=0$ plane but twisted linearly in the spanwise direction. Only small linear twists are allowable, however, in order not to violate the assumptions of small-perturbation linearized theory; hence, the rate of roll is necessarily small (approaching zero).

Pressures on the wing and pressure differences across the wing surface are finite and, for a great variety of plan forms, have already been obtained. (See, for example, refs. 3 and 4.) Off the wing and in the plane of the wing, the pressure, and hence the pressure difference, must be zero.

In the $z=0$ plane, the local pressure difference is directly proportional to the streamwise component of the perturbation velocity and is given simply as

$$\frac{\Delta P(x_1,y_1)}{q}=\frac{2\,\Delta u_s(x_1,y_1)}{V} \tag{1}$$

By consideration of the relationship between the perturbation velocity potential and the streamwise velocity component; that is,

$$\frac{\partial\,\Delta\phi_s(x_1,y_1)}{\partial x_1}=\Delta u_s(x_1,y_1) \tag{2}$$

an expression giving the jump in velocity potential across the xy-plane in terms of the local pressure difference may be written as

$$\Delta\phi_s(x_1,y_1)=\frac{V}{2}\int_{\text{L.E.}}^{x_1}\frac{\Delta P(x,y_1)}{q_0}\,dx \tag{3}$$

Since, from equations (1) and (2),

$$\frac{\Delta P(x_1,y_1)}{q}=\frac{2}{V}\frac{\partial\,\Delta\phi_s(x_1,y_1)}{\partial x_1} \tag{4}$$

and since $\phi_s(x_1,y_1)$ is an odd function in z, it is clear that, beyond the trailing edge, $\Delta\phi_s$ must be independent of x_1 to satisfy the zero-pressure condition in the wake. The integration indicated in equation (3) should, therefore, be made from the wing leading edge to the trailing edge to obtain $\Delta\phi_s$ in the wake.

SOLUTION TO BOUNDARY-VALUE PROBLEM

The linearized partial-differential equation which the perturbation velocity potential must satisfy in supersonic flow is

$$\beta^2\frac{\partial^2\phi}{\partial x^2}-\frac{\partial^2\phi}{\partial y^2}-\frac{\partial^2\phi}{\partial z^2}=0 \tag{5}$$

For the problem being considered herein, the solution to equation (5) may be written as

$$\phi(x,y,z)=-\frac{z\beta^2}{2\pi}\overline{\iint_{\text{Planform}}}\frac{\Delta\phi_s(x_1,y_1)\,dx_1\,dy_1}{[(x-x_1)^2-\beta^2(y-y_1)^2-\beta^2z^2]^{3/2}}-$$

$$\frac{z\beta^2}{2\pi}\overline{\iint_{\text{Wake}}}\frac{\Delta\phi_s(y_1)\,dx_1\,dy_1}{[(x-x_1)^2-\beta^2(y-y_1)^2-\beta^2z^2]^{3/2}} \tag{6}$$

This expression represents the potential in space due to a distribution of doublets in the xy-plane with strengths that are governed by the potential jump across the $z=0$ plane.

The symbol $\overline{\int}$ indicates that the finite parts of the infinite integrals are to be taken when they appear.

APPLICATION TO TRIANGULAR WINGS

The loading over a rolling delta wing with subsonic leading edges has been found in reference 4 to be

$$\frac{\Delta P}{q}(x_1,y_1)=\frac{4px_1\theta_0^3\beta y_1}{V\beta^2G(\theta_0)\sqrt{\theta_0^2x_1^2-\beta^2y_1^2}} \tag{7}$$

where

$$G(\theta_0)=\left[\frac{2-\theta_0^2}{1-\theta_0^2}E'(\theta_0)-\frac{\theta_0^2}{1-\theta_0^2}F'(\theta_0)\right]$$

and

$$E'(\theta_0)=E\left(\frac{\pi}{2},\sqrt{1-\theta_0^2}\right)$$

$$F'(\theta_0)=F\left(\frac{\pi}{2},\sqrt{1-\theta_0^2}\right)$$

From equations (3) and (7) the potential jump across the wing surface is

$$\Delta\phi_s(x_1,y_1)=H\beta y_1\sqrt{\theta_0^2x_1^2-\beta^2y_1^2} \tag{8}$$

and in the wake

$$\Delta\phi_s(y_1)=H\beta y_1\sqrt{\theta_0^2c^2-\beta^2y_1^2} \tag{9}$$

where

$$H=\frac{2p}{\beta^2G(\theta_0)} \tag{10}$$

The velocity potential in space may now be written as the sum of the two expressions (see eq. (6))

$$\phi_P=-\frac{zH\beta^2}{2\pi}\left|\iint_{\text{Plan form}}\frac{\beta y_1\sqrt{\theta_0^2x_1^2-\beta^2y_1^2}dx_1\,dy_1}{[(x-x_1)^2-\beta^2(y-y_1)^2-\beta^2z^2]^{3/2}}\right| \tag{11}$$

and

$$\phi_W=-\frac{zH\beta^2}{2\pi}\left|\iint_{\text{Wake}}\frac{\beta y_1\sqrt{\theta_0^2c^2-\beta^2y_1^2}dx_1\,dy_1}{[(x-x_1)^2-\beta^2(y-y_1)^2-\beta^2z^2]^{3/2}}\right| \tag{12}$$

As previously stated, the primary purpose of this report is the determination of the velocity perturbated behind the wing parallel to the y-axis (or the sidewash). This flow velocity may be obtained by taking the partial derivative of the velocity potential with respect to y, or

$$v=\frac{\partial\phi}{\partial y}$$

With

$$\phi=\phi_P+\phi_W$$

the sidewash in the xz-plane from equations (11) and (12) will be given by the sum of

$$v_P=\left(\frac{\partial\phi_P}{\partial y}\right)_{y\to0}$$

$$=-\lim_{y\to0}\frac{zH\beta^2}{2\pi}\frac{\partial}{\partial y}\left|\iint_{\text{Plan form}}\frac{\beta y_1\sqrt{\theta_0^2x_1^2-\beta^2y_1^2}dx_1\,dy_1}{[(x-x_1)^2-\beta^2(y-y_1)^2-\beta^2z^2]^{3/2}}\right| \tag{13}$$

and

$$v_W=\left(\frac{\partial\phi_W}{\partial y}\right)_{y\to0}$$

$$=-\lim_{y\to0}\frac{zH\beta^2}{2\pi}\frac{\partial}{\partial y}\left|\iint_{\text{Wake}}\frac{\beta y_1\sqrt{\theta_0^2c^2-\beta^2y_1^2}dx_1\,dy_1}{[(x-x_1)^2-\beta^2(y-y_1)^2-\beta^2z^2]^{3/2}}\right| \tag{14}$$

Subsequently it will be convenient for computational purposes to derive expressions for the sidewash which have been nondimensionalized by $pb/2$ so that

$$\frac{v}{pb/2}=\frac{v_P}{pb/2}+\frac{v_W}{pb/2}$$

When $\frac{v}{pb/2}$ is written in a slightly different, though equivalent, form

$$\frac{v/V}{pb/2V}$$

it can be recognized that the nondimensional sidewash parameter may be defined as the induced angle of sidewash per unit wing-tip helix angle $pb/2V$.

The rest of this section is devoted to the evaluation of equations (13) and (14) at points in the following two regions of the xz-plane (see fig. 2):

(1) The region lying between the Mach lines emanating from the wing trailing edge and the line of intersection of the two cones from the trailing-edge tips.

(2) The region which extends from the line of intersection of the two cones from the trailing-edge tips downstream to infinity.

These two regions are denoted, as in reference 1, by E and D, respectively. The contributions of the doublets distributed over the plan form and the wake to the sidewash in regions E and D are considered separately.

Sidewash due to doublets distributed on plan form in region D.—In region D the sidewash contributed by the doublets distributed on the plan form is

$$\frac{\partial\phi_{P,D}}{\partial y}=-\lim_{y\to0}\left(\frac{zH\beta^2}{2\pi}\frac{\partial}{\partial y}\int_0^c\int_{\frac{\theta_0x_1}{\beta}}^{\frac{\theta_0x_1}{\beta}}\frac{\beta y_1\sqrt{\theta_0^2x_1^2-\beta^2y_1^2}dy_1\,dx_1}{[(x-x_1)^2-\beta^2(y-y_1)^2-\beta^2z^2]^{3/2}}\right) \tag{15}$$

In order to facilitate the integrations involved in determining $v_{P,D}$, it is convenient to carry out the differentiation and limiting processes first. This procedure gives

$$v_{P,D}=\frac{3zH\beta^2}{\pi}\int_0^c dx_1\int_0^{\frac{\theta_0x_1}{\beta}}\frac{\beta^3y_1^2\sqrt{\theta_0^2x_1^2-\beta^2y_1^2}dy_1}{[(x-x_1)^2-\beta^2y_1^2-\beta^2z^2]^{5/2}} \tag{16}$$

When the following substitutions are made,

$$s^2=\frac{\beta^2y_1^2}{\theta_0^2x_1^2}$$

$$k_2^2=\frac{\theta_0^2x_1^2}{(x-x_1)^2-\beta^2z^2}$$

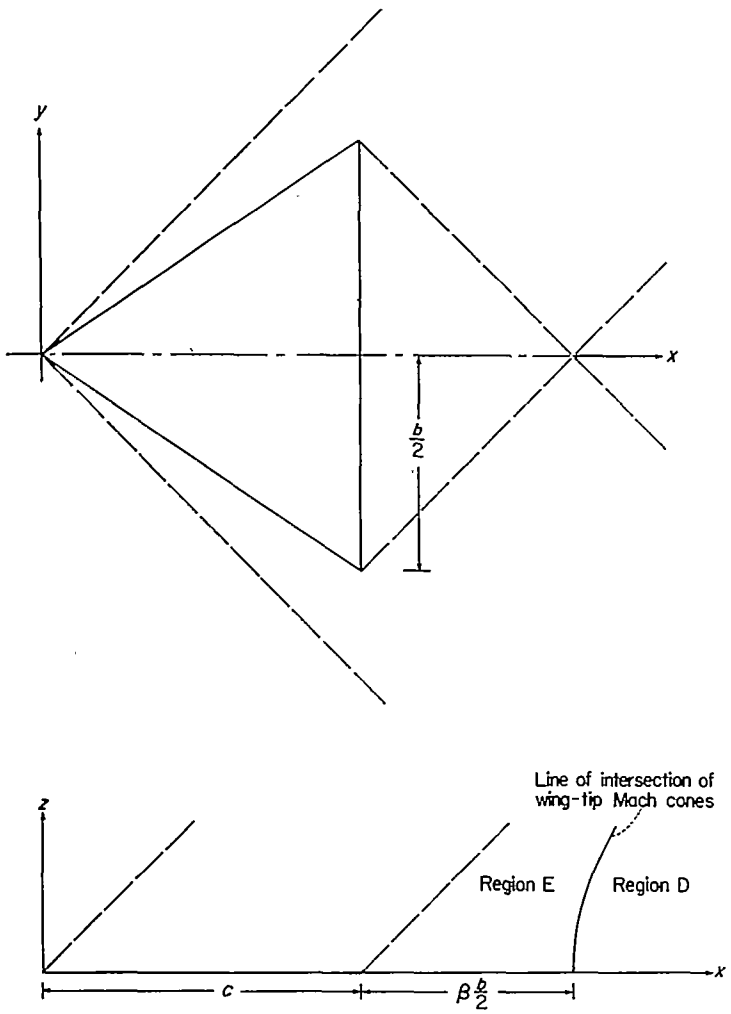

FIGURE 2.—Regions behind a triangular wing.

$v_{P,D}$ becomes

$$v_{P,D}=\frac{3zH\beta^2}{\pi}\int_0^c\frac{k_2^5dx_1}{\theta_0x_1}\int_0^1\frac{s^2\sqrt{1-s^2}\,ds}{(1-k_2^2s^2)^{5/2}} \tag{17}$$

which, by the use of partial fractions, may be written in the more amenable form

$$v_{P,D}=\frac{3zH\beta^2}{\pi}\int_0^c\frac{k_2dx_1}{\theta_0x_1}\left[-\int_0^1\frac{ds}{\sqrt{1-s^2}\sqrt{1-k_2^2s^2}}+(2-k_2^2)\int_0^1\frac{ds}{\sqrt{1-s^2}(1-k_2^2s^2)^{3/2}}-(1-k_2^2)\int_0^1\frac{ds}{\sqrt{1-s^2}(1-k_2^2s^2)^{5/2}}\right] \tag{18}$$

The integrals in equation (18) may be reduced to standard elliptic forms by use of the Jacobian transformation, $s=\mathrm{sn}\,u$ (refs. 5 and 6), and readily integrated to give

$$v_{P,D}=\frac{zH\beta^2}{\pi}\int_0^c\frac{k_2}{\theta_0x_1}\left(-2K_2+\frac{2-k_2^2}{1-k_2^2}E_2\right)dx_1 \tag{19}$$

By replacing H by its equivalent and nondimensionalizing x_1, x, and z, equation (19) becomes

$$\frac{v_{P,D}}{pb/2}=\frac{2z_0}{G(\theta_0)\pi}\int_0^1\frac{k_2}{\theta_0x_{1,0}}\left(-2K_2+\frac{2-k_2^2}{1-k_2^2}E_2\right)dx_{1,0} \tag{20}$$

where

$$k_2^2=\frac{\theta_0^2x_1^2}{(x-x_1)^2-\beta^2z^2}=\frac{\theta_0^2x_{1,0}^2}{(x_0-x_{1,0})^2-\theta_0^2z_0^2}$$

Sidewash due to doublets distributed on plan form in region E.—The portion of the wing area over which the integration in equation (13) is to be performed is different for each position of the field point in region E. This fact is evidenced by the appearance of the field-point coordinates x, y, and z in the limits of integration. It is expedient in determining $v_{P,E}$ to follow the same procedure used in determining $v_{P,D}$ (differentiating before integrating). This is allowable since it can be shown that the expression for the potential $\phi_{P,E}$ can be differentiated with respect to y without regard to the variable limits when the evaluation of the derivative is made at $y=0$.

Differentiating $\phi_{P,E}$ with respect to y and then setting y equal to zero yields

$$v_{P,E}=\frac{3zH\beta}{\pi}\int_0^f dx_1\int_0^{\frac{\theta_0x_1}{\beta}}\frac{y_1^2\sqrt{\frac{\theta_0^2x_1^2}{\beta^2}-y_1^2}\,dy_1}{\left[\frac{(x-x_1)^2-\beta^2z^2}{\beta^2}-y_1^2\right]^{5/2}}+\frac{3zH\beta}{\pi}\sqrt{\int_f^c dx_1\int_0^{\frac{\sqrt{(x-x_1)^2-\beta^2z^2}}{\beta}}\frac{y_1^2\sqrt{\frac{\theta_0^2x_1^2}{\beta^2}-y_1^2}\,dy_1}{\left[\frac{(x-x_1)^2-\beta^2z^2}{\beta^2}-y_1^2\right]^{5/2}}} \tag{21}$$

where

$$f=\frac{x-\sqrt{\theta_0^2x^2+\beta^2z^2(1-\theta_0^2)}}{1-\theta_0^2}$$

The y_1-integration in the first double integral of equation (21) is identical to the y_1-integration in equation (16); hence, only the second term of equation (21) remains to be considered.

In the integration

$$\sqrt{\int_0^{\frac{\sqrt{(x-x_1)^2-\beta^2z^2}}{\beta}}\frac{y_1^2\sqrt{\frac{\theta_0^2x_1^2}{\beta^2}-y_1^2}\,dy}{\left[\frac{(x-x_1)^2-\beta^2z^2}{\beta^2}-y_1^2\right]^{5/2}}}$$

let

$$\frac{\theta_0^2x_1^2}{\beta^2}k_1^2t^2=y_1^2$$

where

$$k_1^2=\frac{(x-x_1)^2-\beta^2z^2}{\theta_0^2x_1^2}$$

This substitution results in the expression

$$\frac{\beta}{\theta_0x_1k_1^2}\sqrt{\int_0^1\frac{t^2\sqrt{1-k_1^2t^2}\,dt}{(1-t^2)^{5/2}}} \tag{22}$$

which, except for the use of the finite-part concept, may be integrated in a manner similar to that used for equation (17). Performing the integration in expression (22) allows $v_{P,E}$

(eq. (21)) to be written as

$$v_{P,E}=\frac{zH\beta^2}{\pi}\int_0^f \frac{dx_1}{\theta_0 x_1} k_2\left(-2K_2+\frac{2-k_2^2}{1-k_2^2}E_2\right)+ \frac{zH\beta^2}{\pi}\int_f^c \frac{dx_1}{\theta_0 x_1}\frac{1}{k_1^2}\left(-K_1+\frac{1-2k_1^2}{1-k_1^2}E_1\right) \tag{23}$$

Equation (23) for $v_{P,E}$ does not lend itself readily to numerical calculations because, at the point $x_1=f$, k_1 and k_2 become equal to 1 and give rise to first-order infinities in the integrands. Appendix A shows how this difficulty is eliminated by a parts integration of the terms containing the singularities. After the singularities have been treated and the x_1-,x-, and z-lengths nondimensionalized, equation (23) becomes

$$\frac{v_{P,E}}{pb/2}=\frac{2z_0}{\pi G(\theta_0)}\left\{\int_0^{f_0}\frac{dx_{1,0}}{\theta_0 x_{1,0}}k_2(-2K_2+E_2)+\int_{f_0}^1\frac{dx_{1,0}}{\theta_0 x_{1,0}}\frac{-K_1+E_1}{k_1^2}-\int_0^{f_0}\frac{\coth^{-1}\left[\frac{-(1-\theta_0^2)x_{1,0}+x_0}{\theta_0\sqrt{x_0^2+z_0^2(1-\theta_0^2)}}\right]}{\theta_0\sqrt{x_0^2+z_0^2(1-\theta_0^2)}}\right.$$
$$\left[\frac{\theta_0(E_2-K_2)}{k_2}-\frac{k_2K_2(x_0-x_{1,0})}{\theta_0 x_{1,0}}\right]dx_{1,0}-\int_{f_0}^1\frac{\tanh^{-1}\left[\frac{-(1-\theta_0^2)x_{1,0}+x_0}{\theta_0\sqrt{x_0^2+z_0^2(1-\theta_0^2)}}\right]}{\theta_0\sqrt{x_0^2+z_0^2(1-\theta_0^2)}}\left[K_1\theta_0-\frac{(E_1-K_1)(x_0-x_{1,0})}{\theta_0 x_{1,0}k_1^2}\right]dx_{1,0}-$$
$$\left.\frac{\pi\sqrt{x_0^2-\theta_0^2z_0^2}}{2\theta_0\sqrt{x_0^2+z_0^2(1-\theta_0^2)}}\coth^{-1}\frac{x_0}{\theta_0\sqrt{x_0^2+z_0^2(1-\theta_0^2)}}+\frac{E_{1,0}}{\sqrt{x_0^2+z_0^2(1-\theta_0^2)}}\tanh^{-1}\frac{-(1-\theta_0^2)+x_0}{\theta_0\sqrt{x_0^2+z_0^2(1-\theta_0^2)}}\right\} \tag{24}$$

where

$$f_0=\frac{x_0-\theta_0\sqrt{x_0^2+z_0^2(1-\theta_0^2)}}{1-\theta_0^2}$$

Numerical calculations may be made by using equation (24) for all values of θ_0 except $\theta_0=1$ where f_0 becomes indeterminate and the arc hyperbolic functions become infinite. The indeterminacy when evaluated yields

$$(f_0)_{\theta_0=1}=\frac{x_0^2-\theta_0^2z_0^2}{2x_0}$$

Thus, an integration by parts of the singular terms of equation (23) similar to that made to obtain equation (24), using now $(f_0)_{\theta_0=1}$ and expressions for k_1 and k_2 in which θ_0 has been set equal to 1, yields

$$\frac{v_{P,E}}{pb/2}=\frac{2z_0}{\pi G(\theta_0)}\left\{\int_0^{f_0}\frac{dx_{1,0}}{x_{1,0}}k_2(-2K_2+E_2)+\int_{f_0}^1\frac{dx_{1,0}}{x_{1,0}k_1^2}(-K_1+E_1)+\frac{1}{2x_0}\int_0^{f_0}-\log_e(-2x_0x_{1,0}+x_0^2-z_0^2)\left[\frac{E_2-K_2}{k_2}-\frac{k_2K_2(x_0-x_{1,0})}{x_{1,0}}\right]dx_{1,0}+\right.$$
$$\frac{1}{2x_0}\int_{f_0}^1\log_e(2x_0x_{1,0}-x_0^2+z_0^2)\left[K_1-\frac{(E_1-K_1)(x_0-x_{1,0})}{k^2x_{1,0}}\right]dx_{1,0}-\frac{E_1(k_1=\sqrt{(x_0-1)^2-z_0^2})}{2x_0}\log_e(2x_0-x_0^2+z_0^2)+$$
$$\left.\frac{\pi\sqrt{x_0^2-z_0^2}}{4x_0}\log_e(x_0^2-z_0^2)\right\} \tag{25}$$

The integrations in equation (25) may be handled by numerical methods.

Sidewash due to doublets distributed in wake in region D.—In region D, equation (14) takes the form

$$v_{W,D}=\lim_{y\to 0}\left\{-\frac{zH\beta^2}{2\pi}\frac{\partial}{\partial y}\left|\int_{-\frac{\theta_0 c}{\beta}}^{\frac{\theta_0 c}{\beta}}\beta y_1\sqrt{\theta_0^2c^2-\beta^2y_1^2}\,dy_1\int_c^{x-\beta\sqrt{(y-y_1)^2+z^2}}\frac{dx_1}{[(x-x_1)^2-\beta^2(y-y_1)^2-\beta^2z^2]^{3/2}}\right|\right\} \tag{26}$$

Carrying out the differentiation and then the first integration for $y=0$ gives

$$v_{W,D}=\frac{zH(x-c)}{\pi\beta^2}\int_0^{\frac{\theta_0 c}{\beta}}\left\{\frac{3\beta^2y_1^2\sqrt{\theta_0^2c^2-\beta^2y_1^2}}{(y_1^2+z^2)\,[(x-c)^2-\beta^2y_1^2-\beta^2z^2]^{1/2}}-\frac{(x-c)^2\beta^2y_1^2\sqrt{\theta_0^2c^2-\beta^2y_1^2}}{(y_1^2+z^2)^2\,[(x-c)^2-\beta^2y_1^2-\beta^2z^2]^{3/2}}\right\}d(\beta y_1) \tag{27}$$

By making the variable substitution

$$y_1^2=s^2\frac{\theta_0^2c^2}{\beta^2}$$

and defining

$$\frac{\theta_0^2c^2}{(x-c)^2-\beta^2z^2}=k_{2,0}^2$$

equation (27) reduces to

$$v_{W,D}=\frac{3H(x-c)\theta_0^3c^3k_{2,0}}{\pi\beta^2z^3}\int_0^1\frac{s^2\sqrt{1-s^2}\,ds}{\left(1+\frac{\theta_0^2c^2}{z^2\beta^2}s^2\right)^2\sqrt{1-k_{2,0}s^2}}-$$

$$\frac{H(x-c)^3\theta_0ck_{2,0}^3}{\pi\beta^2z^3}\int_0^1\frac{s^2\sqrt{1-s^2}\,ds}{\left(1+\frac{\theta_0^2c^2}{z^2\beta^2}s^2\right)^2(1-k_{2,0}^2s^2)^{3/2}} \tag{28}$$

The expression for $v_{W,D}$ given by equation (28) may be integrated (see appendix B) to yield a closed-form solution for $v_{W,D}$. The nondimensional equation for $\frac{v_{W,D}}{pb/2}$ is

$$\frac{v_{W,D}}{pb/2}=\frac{2}{\pi G(\theta_0)}\left\{\left[\frac{\pi}{2}+(K_{2,0}-E_{2,0})F\left(\cot^{-1}\frac{1}{z_0},k_{2,0}'\right)-\right.\right.$$

$$\left.\left.K_{2,0}E\left(\cot^{-1}\frac{1}{z_0},k_{2,0}'\right)\right]\frac{2z_0^2+1}{\sqrt{z_0^2+1}}-\frac{K_{2,0}k_{2,0}(x_0-1)z_0}{\theta_0(z_0^2+1)}\right\} \tag{29}$$

Sidewash due to doublets distributed in wake of region E.—In region E the derivation of the sidewash is similar to that of region D and yields

$$\frac{v_{W,E}}{pb/2}=\frac{2(x_0-1)}{\pi\theta_0G(\theta_0)}\left\{\left[\frac{\pi}{2}+\frac{K_{1,0}\theta_0z_0\sqrt{z_0^2+1}}{x_0-1}+\right.\right.$$

$$(K_{1,0}-E_{1,0})F\left(\cot^{-1}\frac{k_{1,0}}{z_0},k_{1,0}'\right)-$$

$$\left.\left.K_{1,0}E\left(\cot^{-1}\frac{k_{1,0}}{z_0},k_{1,0}'\right)\right]\frac{(2z_0^2+1)\theta_0}{\sqrt{z_0^2+1}\,(x_0-1)}-2K_{1,0}z_0\right\} \tag{30}$$

where

$$k_{1,0}^2=\frac{(x-c)^2-\beta^2z^2}{\theta_0^2c^2}$$

Sidewash at x-axis.—In the xy-plane (plane of the wake), only the doublets distributed in the wake contribute to the sidewash. Equation (20) for $\frac{v_{P,D}}{pb/2}$ and equations (24) and (25) for $\frac{v_{P,E}}{pb/2}$ approach zero as z_0 approaches zero, whereas equations (29) and (30) give

$$\frac{v_{W,D}}{pb/2}=\frac{v_{W,E}}{pb/2}=\frac{1}{G(\theta_0)} \tag{31}$$

This result is identical with that which would be obtained by use of the formula obtained in reference 7 by considering the properties of vortex sheets. This formula, for $y=y_1=0$, is

$$\frac{v}{pb/2}(x,0,0^+)=\frac{1}{2\frac{pb}{2}}\left(\frac{d\Gamma}{dy_1}\right)_{y_1=0} \tag{32}$$

where

$$\Gamma=(\Delta\phi_s)_{TE} \tag{33}$$

Sidewash at $x=\infty$ (Trefftz plane).—As x approaches infinity, the contribution of the doublets distributed on the plan form to the sidewash goes to zero and the total sidewash is given by

$$\left(\frac{v_{W,D}}{pb/2}\right)_{x\to\infty}=\left(\frac{v}{pb/2}\right)_{x\to\infty}=\frac{1}{G(\theta_0)}\left(\frac{1+2z_0^2}{\sqrt{1+z_0^2}}-2z_0\right) \tag{34}$$

Equation (34) could also have been determined more directly by using the formula

$$\left(\frac{v}{pb/2}\right)_{x\to\infty}=\lim_{y\to0}\frac{z}{2\pi pb/2}\left[\frac{\partial}{\partial y}\int_{-b/2}^{b/2}\frac{\Delta\phi_s(x_{TE},y_1)dy_1}{(y-y_1)^2+z^2}\right] \tag{35}$$

which may be obtained from equation (26) by performing the first integration and then setting x equal to infinity.

LIFTING-LINE SIDEWASH

The lifting-surface method by which the sidewash behind a rolling delta wing was derived in the previous section is applicable to wings of arbitrary plan form; however, the integrations which would be required before the potential or one of the perturbation velocities could be obtained in a calculable form are extremely difficult to evaluate. It is of importance, therefore, to develop some approximate expressions which may be easily evaluated either analytically or numerically. References 2 and 8 indicate that a lifting line and a lifting line approximated by supersonic horseshoe vortices can be used as good approximations to lifting-surface solutions for most downwash problems. It would seem that a comparison of the sidewash behind the rolling delta wing calculated by the lifting-surface method with that calculated by an approximate method might give some indication of the usefulness of the "approximate" approach for sidewash problems.

References 2 and 8 together represent a fairly thorough study of the lifting-line and approximate lifting-line methods, especially with regard to downwash calculations, and show that the swept lifting lines will probably give the best results for swept and triangular wings. The potential due to a yawed lifting line may be obtained from the errata of reference 2 as

$$\phi=\frac{\Gamma(y_1)}{2\pi}\tan^{-1}\frac{z\sqrt{X^2-\beta^2(Y^2+z^2)}}{YX-\frac{z^2}{m}\frac{Y^2}{m}}\Bigg|_{h_1}^{h_2}-$$

$$\frac{1}{2\pi}\int_{h_1}^{h_2}\frac{d\Gamma(y_1)}{dy_1}\tan^{-1}\frac{z\sqrt{X^2-\beta^2(Y^2+z^2)}}{YX-\frac{z^2}{m}\frac{Y^2}{m}}dy_1 \tag{36}$$

where the equation of the lifting line is

$$x_1=\frac{y_1+k}{m}$$

and the circulation Γ is defined by equation (33) as the potential jump across the surface evaluated at the trailing edge. (See fig. 3.) When $\frac{d\Gamma(y_1)}{dy_1}$ is zero, equation (36) becomes

$$\phi=\frac{\Gamma}{2\pi}\tan^{-1}\frac{z\sqrt{X^2-\beta^2(Y^2+z^2)}}{YX-\frac{z^2}{m}\frac{Y^2}{m}}\Bigg|_{h_1}^{h_2} \tag{37}$$

which might be considered as the potential in space (at a point x, y, z) of a finite yawed vortex of constant strength. A number of finite yawed vortices distributed along a line can be used to approximate the potential in space of a lifting line with any prescribed lift distribution.

From equation (37), the sidewash due to a yawed vortex is readily obtained by taking the derivative with respect to y. The following result is obtained:

$$v=\frac{\partial\phi}{\partial y}=\frac{\Gamma}{2\pi}\left\{\frac{\frac{zY}{m}(2X^2-\beta^2Y^2-\beta^2z^2)-zX(X^2-\beta^2z^2)}{\sqrt{X^2-\beta^2(Y^2+z^2)}\left[\left(YX-\frac{z^2}{m}-\frac{Y^2}{m}\right)^2+z^2(X^2-\beta^2Y^2-\beta^2z^2)\right]}\right\}_{h_1}^{h_2} \tag{38}$$

When m approaches infinity, equation (38) becomes the sidewash for a rectangular horseshoe vortex and agrees with the equations given in references 9 and 10.

Since the loading on a rolling wing is antisymmetrical, the induced sidewash from each panel is in the same direction and equal in the $y=0$ plane. For this reason it is necessary to calculate the sidewash only from one panel and double it.

Equation (38) can be utilized to formulate an approximate expression for the sidewash due to a series of constant-strength yawed horseshoe vortices spaced along a line so as to represent as closely as possible the span load distribution due to rolling. This expression is

$$v=-\sum_{i=0}^{n}\frac{\Gamma(y_{i+1})-\Gamma(y_{i-1})}{4\pi}\frac{\frac{zY_i}{m}(2X_i^2-\beta^2Y_i^2-\beta^2z^2)-zX_i(X_i^2-\beta^2z^2)}{\sqrt{X_i^2-\beta^2Y_i^2-\beta^2z^2}\left[\left(Y_iX_i-\frac{z^2}{m}-\frac{Y_i^2}{m}\right)^2+z^2(X_i^2-\beta^2Y_i^2-\beta^2z^2)\right]} \tag{39}$$

where $Y_i=y-y_i$, $X_i=x-x_i$, and $x_i=\frac{y_i+k}{m}$, the subscript i takes on all integral values from 0 to n. Equation (39) in nondimensional form is

$$\frac{v}{vb/2}=-\sum_{i=0}^{n}\frac{\left[\frac{\Gamma(y_{i+1})}{p(b/2)^2}-\frac{\Gamma(y_{i-1})}{p(b/2)^2}\right]\left[\frac{z_0Y_{i,0}}{m}(2\overline{X}_i^2-\beta^2Y_{i,0}^2-\beta^2z_0^2)-z_0\overline{X}_i(\overline{X}_i^2-\beta^2z_0^2)\right]}{4\pi\sqrt{\overline{X}_i^2-\beta^2Y_{i,0}^2-\beta^2z_0^2}\left[\left(Y_{i,0}\overline{X}_i-\frac{z_0^2}{m}-\frac{Y_{i,0}^2}{m}\right)^2+z_0^2(\overline{X}_i^2-\beta^2Y_{i,0}^2-\beta^2z_0^2)\right]} \tag{40}$$

In the application of equation (40) to the calculation of sidewash, some care should be exercised that the forecone from the field point under consideration does not intersect the lifting line at a point close to the corner of a yawed horseshoe vortex. When the forecone intersects the lifting line near a corner located within the forecone, the expression under the radical in the denominator of equation (40) becomes small and the sidewash becomes large. (See sketch 1.) A zero value for the square root and an infinite value for the sidewash result when the forecone intersects the corner. The abruptness of the infinity varies with the distance of the field point from the corner. Note that when $x=\infty$, the infinity no longer exists. The preferable field-point locations have forecones intersecting the lifting line as shown in sketch 2. The closeness of the

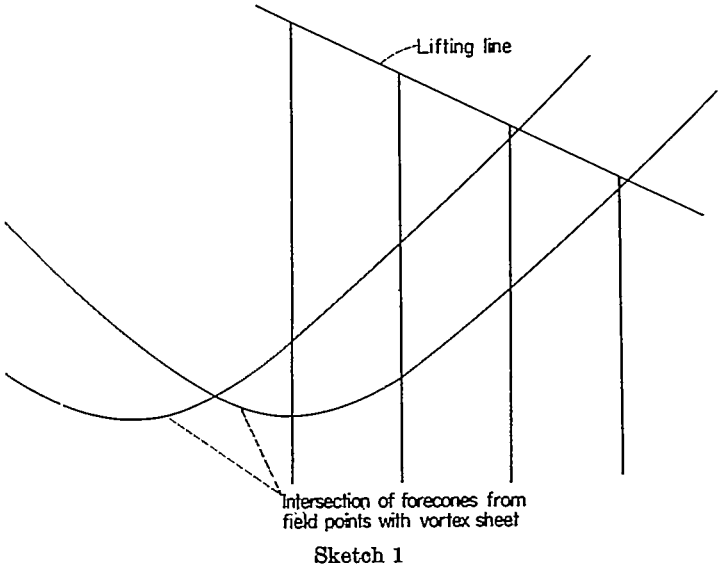

Sketch 1

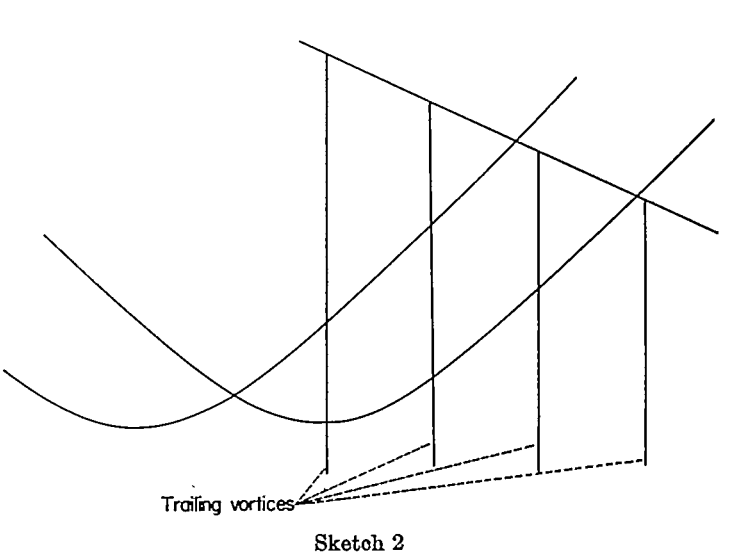

Sketch 2

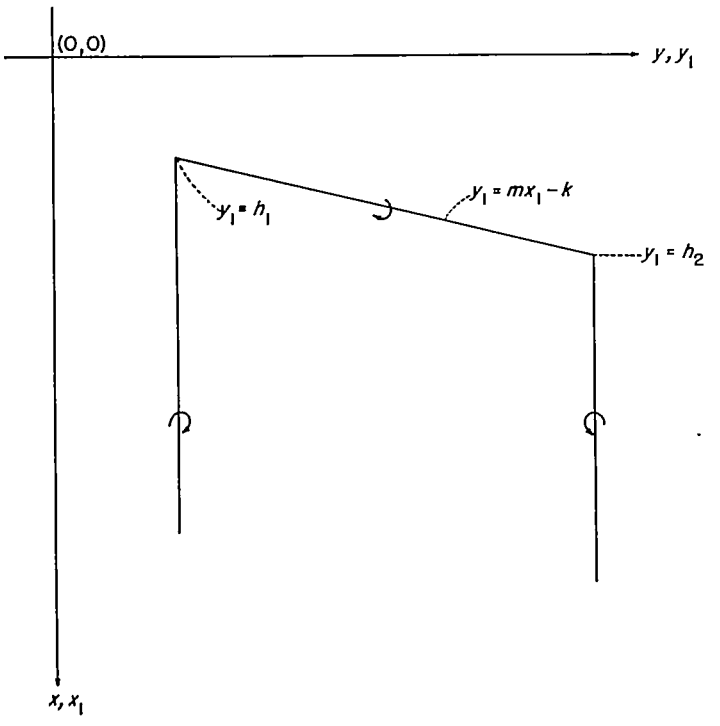

FIGURE 3.—Finite yawed vortex used to approximate a swept lifting line.

forecone to the corner when the corner is outside the Mach cone is obviously of no consequence because only line vortices within the forecone from the field point contribute to the sidewash at the point.

RESULTS AND DISCUSSION

EXACT SIDEWASH

The exact linearized nondimensional sidewash has been calculated for values of θ_0 of 1.00, 0.75, 0.50, 0.40, and 0.30; values of x_0 from 1.2 to 2.4; and values of z_0 from 0 to 0.6 except where these values are ahead of region E. Variations of the sidewash parameter $\frac{v/V}{pb/2V}$ with x_0 for 7 values of z_0 from 0 to 0.6 and for the θ_0's given are presented in figure 4. Cross plots of figure 4 which show the variation of the sidewash parameter with z_0 for 7 values of x_0 from 1.2 to 2.4 are given as figure 5.

In order to depict the effect of Mach number and leading-edge sweep, variations of the sidewash parameter with z_0 for values of θ_0 of 1.00, 0.75, 0.50, and 0.30 have been plotted for three longitudinal locations: $x_0=1.6$, $x_0=2.0$, and $x_0=\infty$ (fig. 6). (It should be noted at this point that an increase in θ_0 may be interpreted as either an increase in Mach number for a fixed leading-edge slope or an increase in the wing semiapex angle for a specific Mach number.) The major difference to be noted in the effects of changing θ_0 is that, when the longitudinal station is ahead of the line of intersection of the Mach cones from the trailing-edge tips, an increase in θ_0 causes an increase in the sidewash at the higher values of z_0, whereas the sidewash at a station remaining behind the intersection line during an increase in θ_0 experiences a decrease in sidewash at all values of z_0 which are unaffected by the localized infinity at the intersection line. By way of illustration it can be seen at station $x_0=1.6$ that

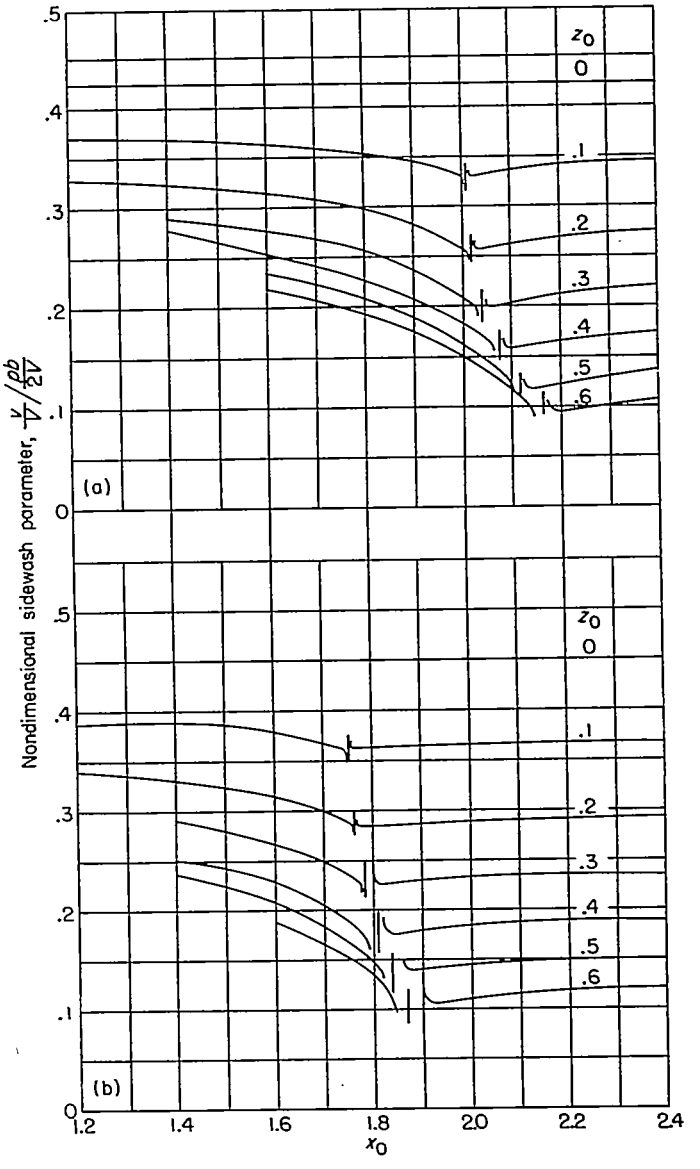

(a) $\theta_0=1.00$.

(b) $\theta_0=0.75$.

FIGURE 4.—Longitudinal variation of nondimensional sidewash parameter $\frac{v/V}{pb/2V}$ in x_0z_0-plane behind triangular wing for a number of values of z_0 and θ_0.

when θ_0 is increased from 0.75 to 1.00 the sidewash increases for values of z_0 greater than 0.2; for values of θ_0 of 0.3 and 0.5, when $x_0=1.6$ is behind the intersection line, the effect of increasing θ_0 is to decrease the sidewash at all values of z_0 except at $z_0=0.6$. This point is affected by the infinity at the intersection line.

APPROXIMATE SIDEWASH

From the nature of the analytical and numerical integrations required to obtain the exact sidewash for triangular wings, it is apparent that for wings with more complex potential-jump expressions the derivation of exact sidewash would be a difficult task. Herein lies the merit of the approximate lifting-line method (eq. (40)) which is not encumbered by the complexity of the wing-loading expression.

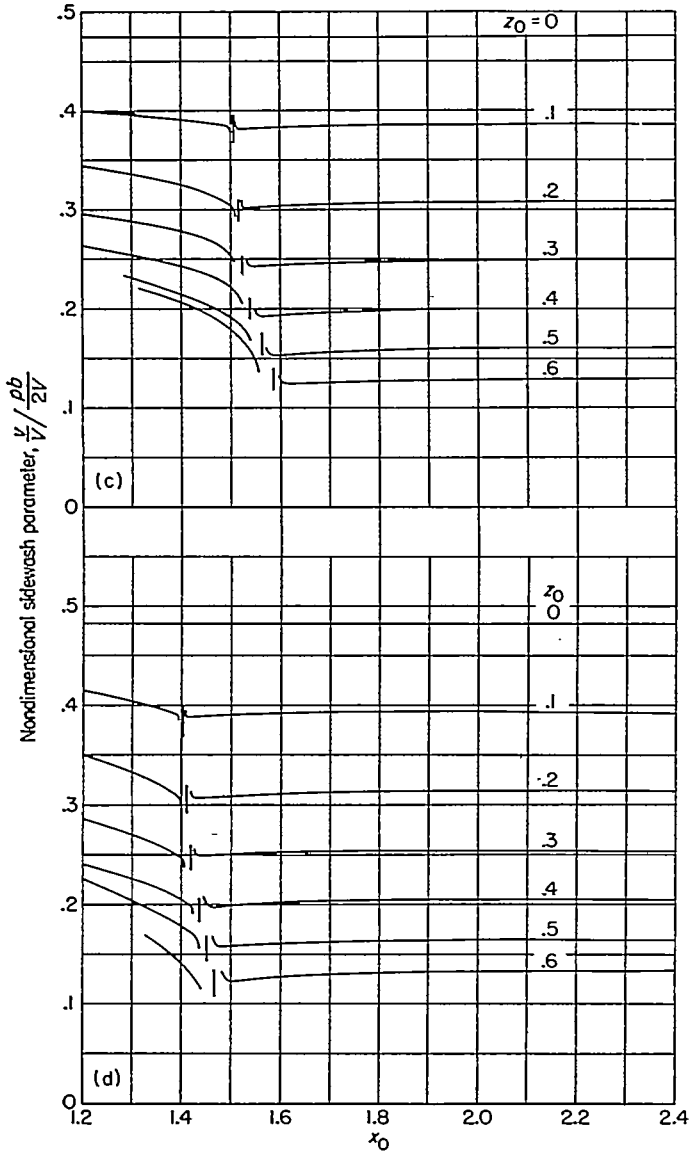

(c) $\theta_0 = 0.50$.

(d) $\theta_0 = 0.40$.

FIGURE 4.—Continued.

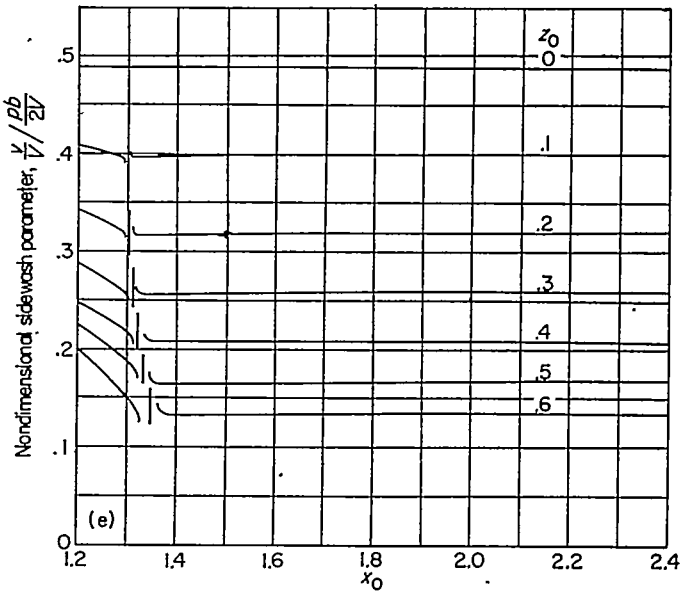

(e) $\theta_0 = 0.30$.

FIGURE 4.—Concluded.

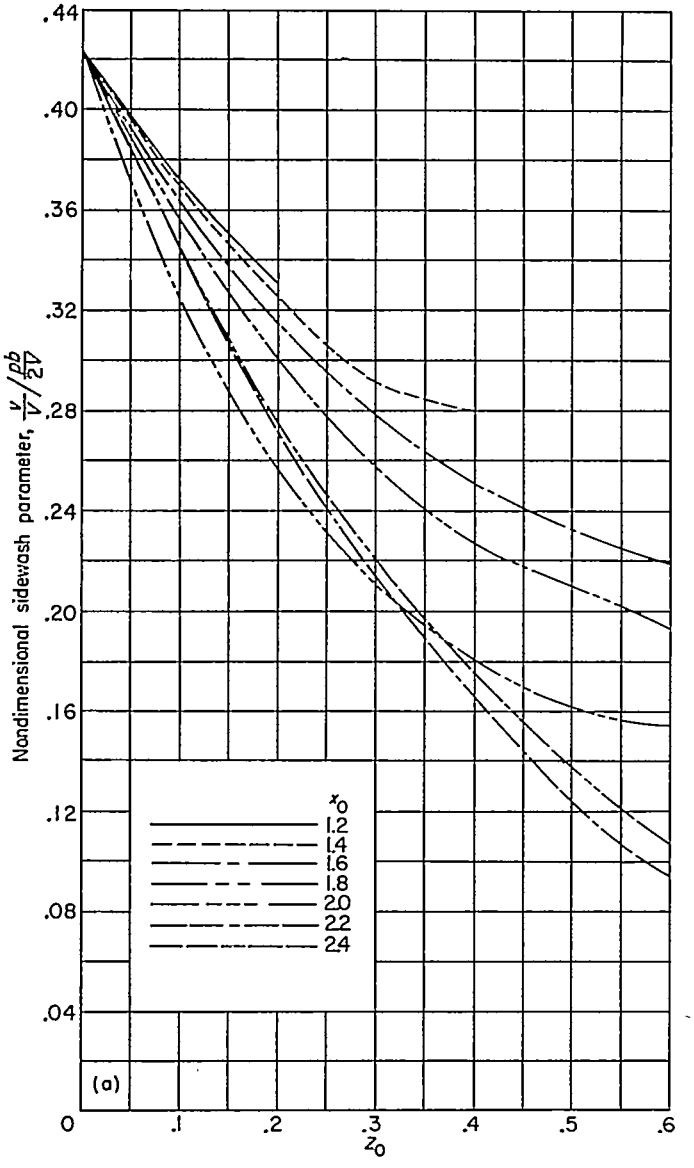

(a) $\theta_0=1.00$.

FIGURE 5.—Variation with z_0 of nondimensional sidewash parameter in x_0z_0-plane at a number of longitudinal stations.

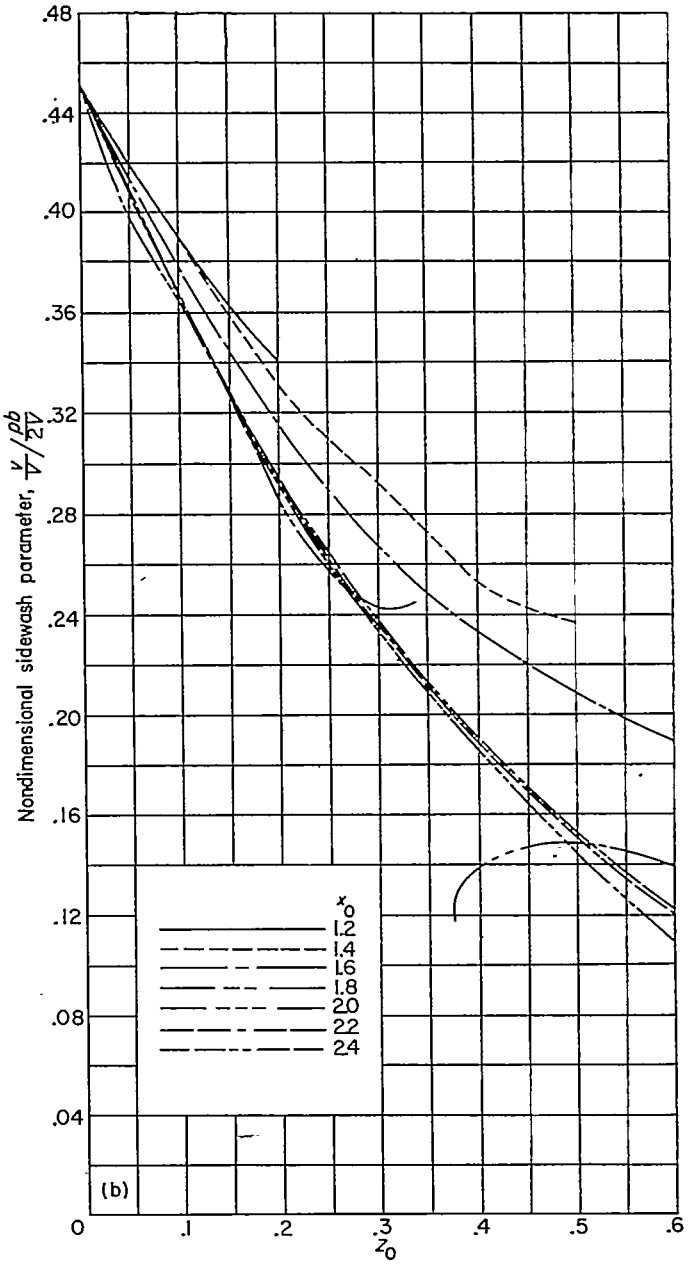

(b) $\theta_0=0.75$.

FIGURE 5.—Continued.

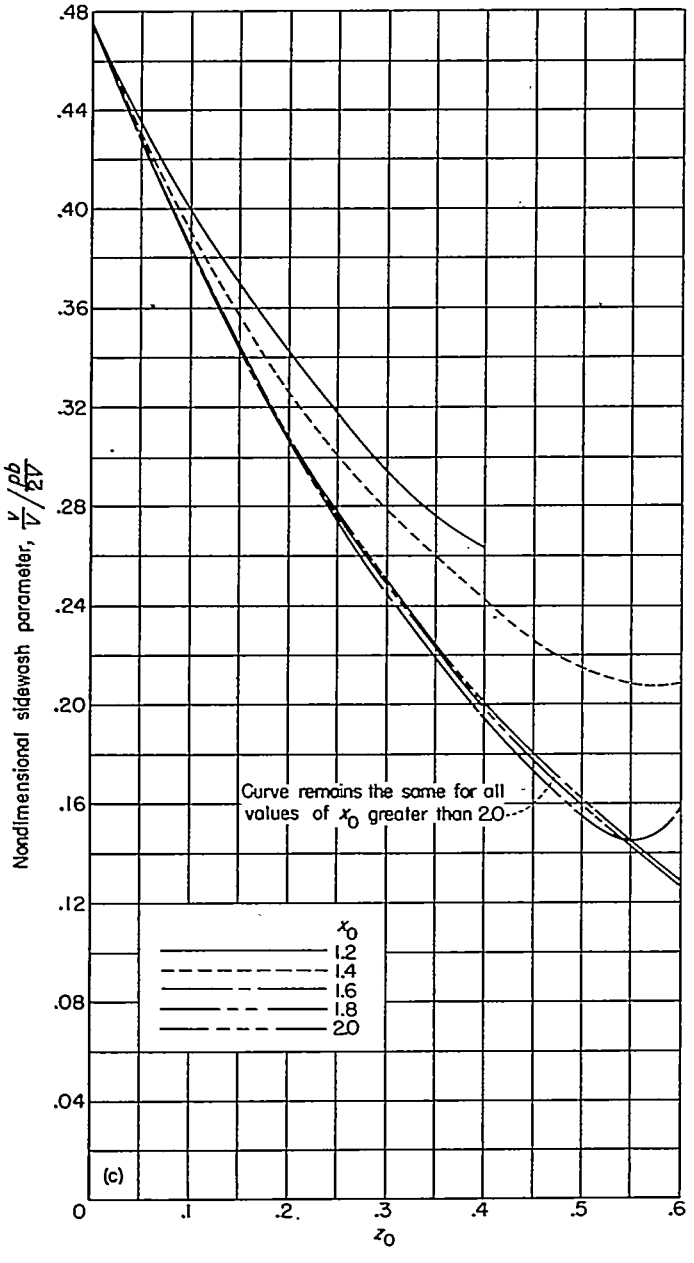

(c) θ_0=0 50.

FIGURE 5.—Continued.

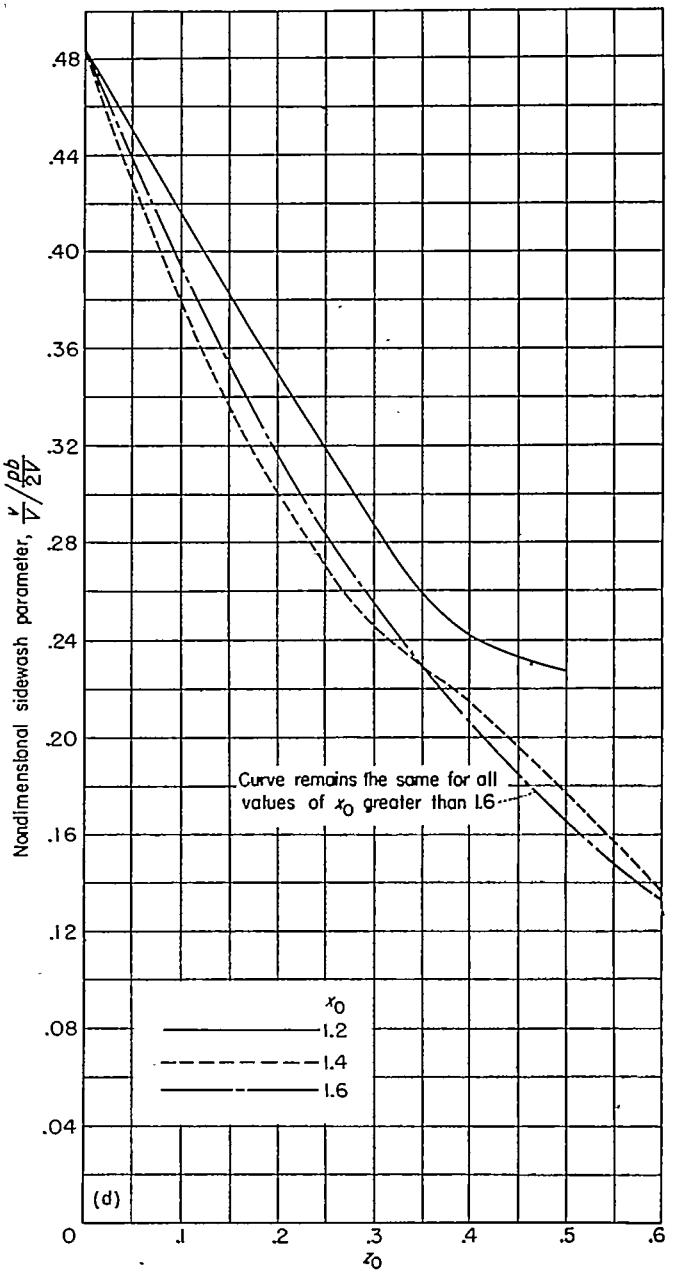

(d) θ_0=0.40.

FIGURE 5.—Continued.

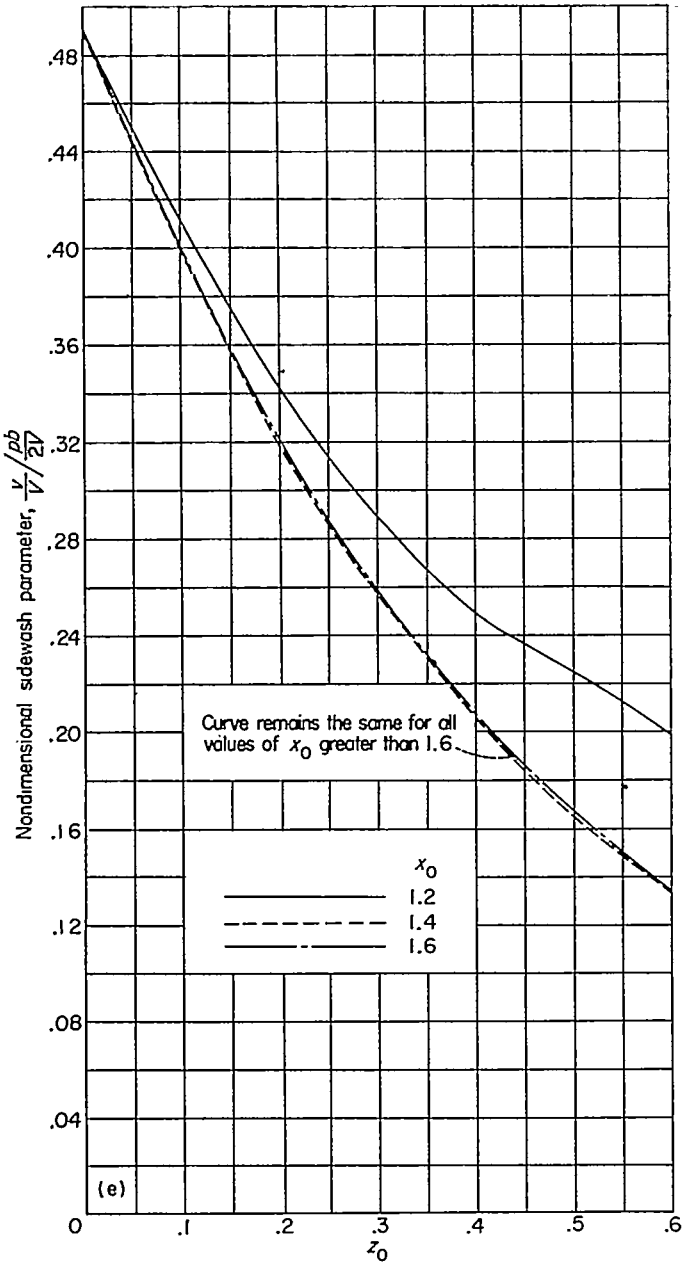

(e) $\theta_0=0.30$.

FIGURE 5.—Concluded.

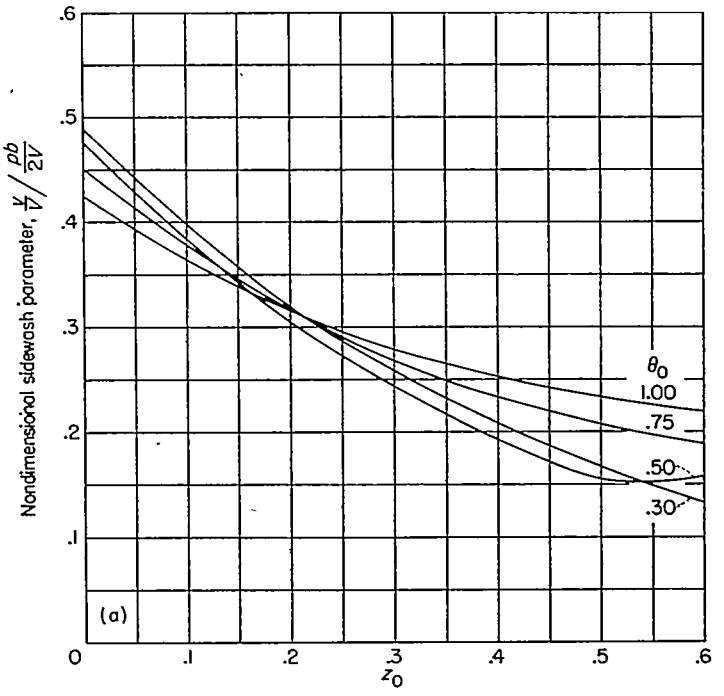

(a) $x_0=1.6$.

FIGURE 6.—Change in vertical variation of sidewash with θ_0 at $x_0=1.6$, 2.0, and infinity.

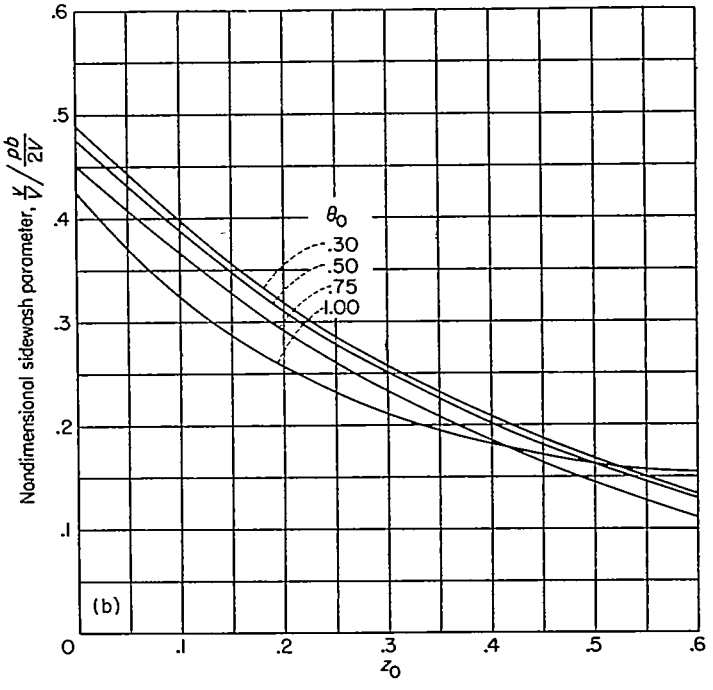

(b) $x_0=2.0$.

FIGURE 6.—Continued.

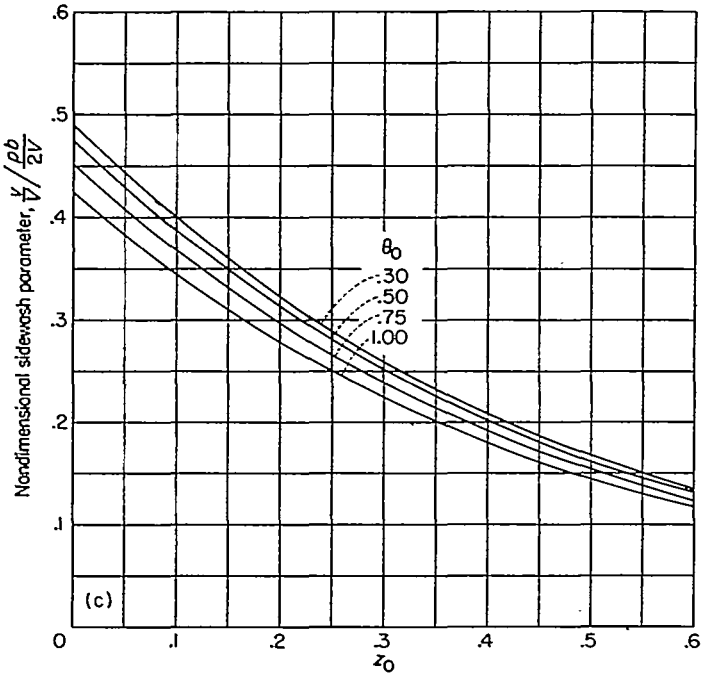

(c) $x_0=\infty$.

FIGURE 6.—Concluded.

The approximate method is, however, hindered to the extent that an area distribution of loading is assumed concentrated on one or several lines. The penalty that this assumption imposes on the quality of the results cannot be ascertained in every case. For the triangular wing treated herein, comparisons may be made between the results from the lifting-line and the lifting-surface methods, and perhaps some indication may be obtained as to the regions wherein the approximate method may or may not give reliable values.

By use of equation (40), approximate lifting-line calculations of the sidewash have been made for $\theta_0=1.00$ and 0.40, values of x_0 from 1.2 to 2.4, and values of z_0 from 0.1 to 0.6. Sidewash values for $z_0=0$ were obtained from equation (32). A comparison of the sidewash calculated by the lifting-line and lifting-surface methods has been made in figure 7, and the agreement is shown to be good everywhere except at the high values of z_0 close behind the trailing edge for $\theta_0=1.00$. The agreement in this region is considerably better at $\theta_0=0.40$ (fig. 7(b)) and indicates that as θ_0 is decreased from 1.00 the approximate calculations will become more reliable at locations close behind the trailing edge.

Seventeen yawed horseshoe vortices were used to approximate the lifting line, with the concentration of vortices greater near the tip because of the rapid change in the span loading in this region. The lifting line used in the approximate calculations consisted of a pair of straight lines connecting the midpoint of the root chord to the tips. Additional computations of the sidewash have been made using lifting lines composed of straight lines connecting the tips with the $c/4$ point and connecting the tips with the $3c/4$ point but the agreement with the exact sidewash was not so good as that evidenced in figure 7.

It is of interest that the spanwise center of loading of the loading distributed along the lifting line connecting the $c/2$ point with the tips (the lifting line yielding the best agreement with the lifting-surface results) was located longitudinally closer to the actual wing center of loading at $3c/4$ than it was when the loading was distributed on the other two lifting lines.

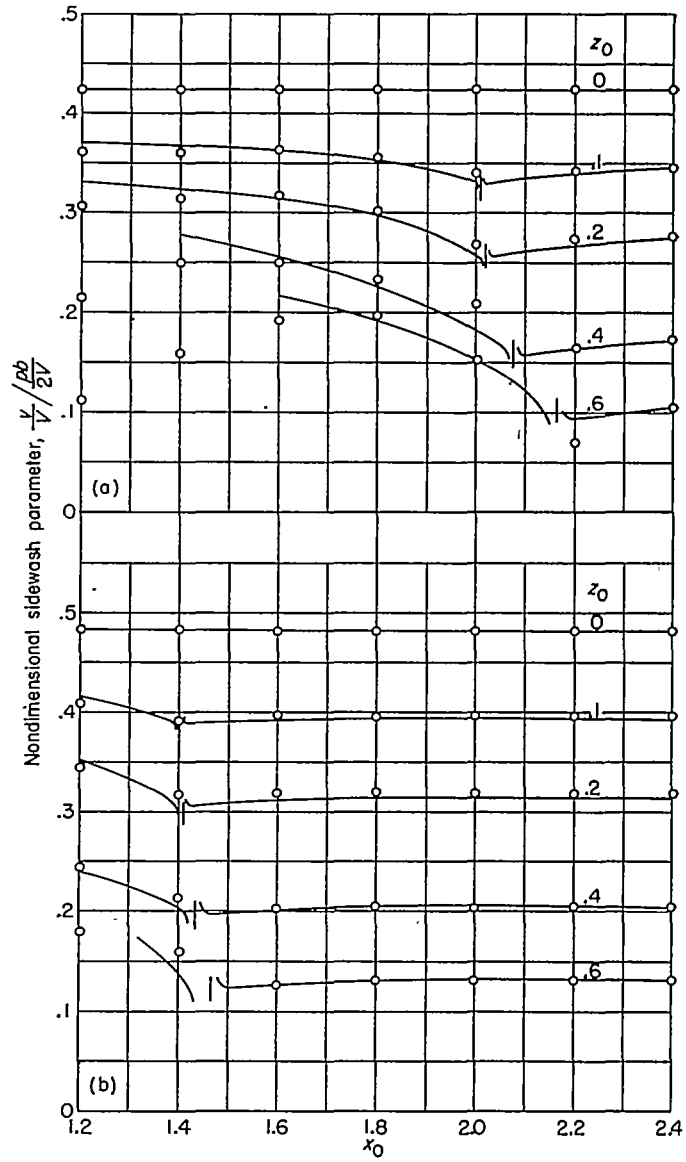

(a) $\theta_0=1.00$.
(b) $\theta_0=0.40$.

FIGURE 7.—Comparison of lifting-line and lifting-surface sidewash for $\theta_0=1.00$ and 0.40. Circles represent points calculated by lifting-line method.

The wing loading in the examples just discussed was distributed on one lifting line. Sidewash obtained by distributing the wing loading on more than one lifting line would probably show better agreement with the exact results in region E, because some effect of the longitudinal distribution of loading over the wing could then be realized.

EXAMPLE OF FLOW-FIELD EFFECT ON VERTICAL TAIL

The effect of the induced sidewash velocity behind a rolling wing on the forces and moments contributed by a vertical tail can best be illustrated by analyzing a specific wing-tail configuration. The pertinent geometric characteristics of the wing-tail model are (see fig. 8):

Wing aspect ratio	3.2
Tail aspect ratio	1.866
$\frac{\text{Tail area}}{\text{Wing area}}$	0.21
$\frac{\text{Tail span}}{\text{Wing semispan}}$	0.7
$\frac{\text{Tail chord}}{\text{Wing chord}}$	0.6
Center-of-gravity location	0.5c

A free-stream Mach number of 1.6 (β=1.25) has been chosen. The wing leading edge for this Mach number is sonic (θ_0=1) and the vertical-tail leading edge is supersonic. Induced side-force and yawing moments for a number of longitudinal positions of the vertical tail have been determined by numerical integrations in a manner similar to that used in reference 11 to obtain the contribution of horizontal tails with supersonic leading edges to the lift and pitching moment. In making the numerical integrations, sidewash curves (figs. 4 and 5) were used which had the infinity at the tip-cone intersection line faired through. Isolated vertical-tail forces and moments have been computed from the formulas given in reference 12.

Figure 9 shows in stability-derivative form the variation of the induced, isolated, and total forces and moments with the longitudinal location of the vertical tail. For the example configuration chosen, the induced forces and moments are greater than the "isolated" forces and give rise to a positive C_{Y_p} coefficient and a negative C_{n_p}. Obviously, from the sidewash curves, if the vertical tail were moved away from the x-axis, the induced force would be reduced. The isolated forces and moments, on the other hand, would increase and the total C_{Y_p} and total C_{n_p} would become negative and positive, respectively.

ASSUMPTIONS AND LIMITATIONS

In some cases, the assumptions made in the analysis, by necessity or for convenience, to allow the determination of the sidewash behind triangular wings by linearized supersonic flow theory limit the application of the results. Some discussion of these assumptions and limitations may be useful.

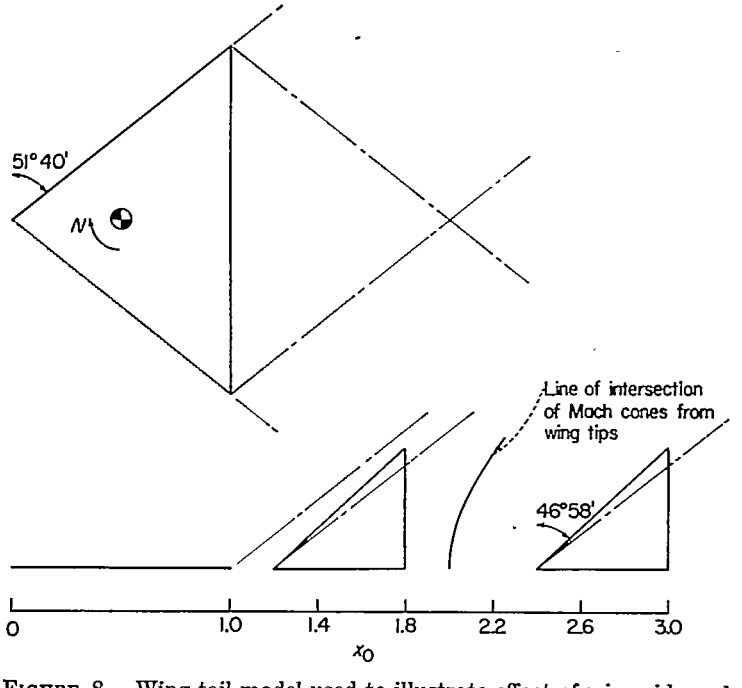

FIGURE 8.—Wing-tail model used to illustrate effect of wing sidewash on a vertical tail.

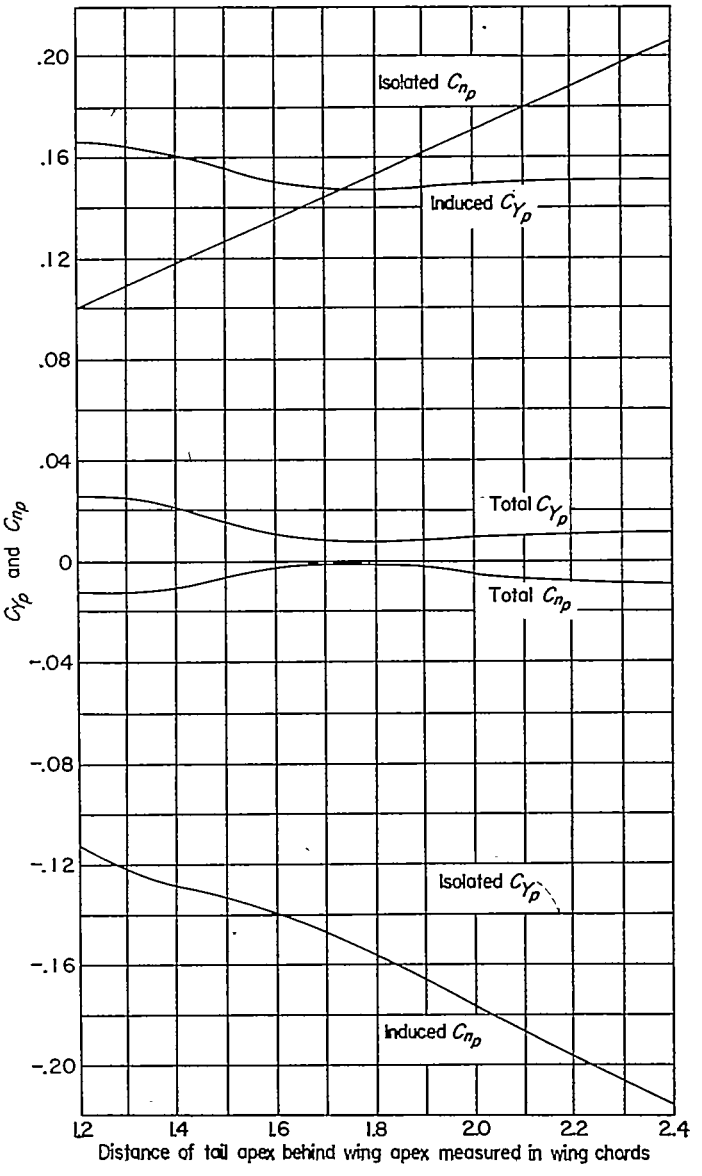

FIGURE 9.—Variation of induced, isolated, and total forces and moments (in stability-derivative form) with longitudinal location of vertical tail.

The validity of the assumption of a flat vortex sheet for wings with very low aspect ratios is questionable, but, in the absence of experimental and theoretical information directly concerned with the vortex sheet behind rolling wings, no definite statement can be made as to the effects that wing aspect ratio, roll velocity, and distance behind the trailing edge will have on the rolling-up of the vortex sheet. It may be possible, as suggested in reference 13, to get some indication of these effects from the data published in references 14 and 15 concerning the rolling-up of the vortex sheet behind wings at an angle of attack.

The vortex sheet has been assumed not to rotate. The angle (in degrees) through which the vortex sheet would rotate in moving from the wing trailing edge to a point d

distance downstream is given by

$$\lambda=\frac{180}{\pi}\frac{pd}{V}$$

$$=\frac{180}{\pi}\frac{pb}{2V}\left(\frac{d}{b/2}\right)$$

Substitution into this formula of values of $pb/2V$ usually encountered and of distance d up to two semispans will generally yield rotation angles small enough to be neglected.

The sidewash expressions derived in the analysis for rolling wings at zero angle of attack are also applicable for finite angles of attack because angle-of-attack loadings are symmetrical and do not contribute to the sidewash in the xz-plane. The displacement of the assumed flat vortex sheet from its zero angle-of-attack position, however, must be accounted for; that is, the sidewash given for a point $x, z=0^+$ for the zero angle-of-attack case represents the sidewash at the vortex sheet when the wing is at an angle of attack. At a distance d behind the trailing edge, the displacement of the vortex sheet below the trailing edge may be found (see sketch 3) from

$$h=\int_{\text{T.E.}}^{d}\tan\epsilon\,dx$$

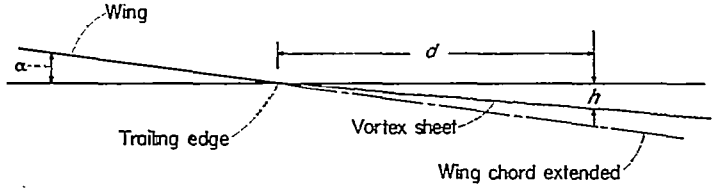

Sketch 3

Values of tan ϵ for a triangular wing are given in reference 2.

CONCLUDING REMARKS

The variation of sidewash with longitudinal distance in the vertical plane of symmetry behind rolling triangular wings traveling at supersonic speeds has been derived by linearized lifting-surface and lifting-line methods. The range of supersonic Mach numbers for which the lifting-surface results are valid is limited by the condition that the wing leading edges must be subsonic. The variations of lifting-surface sidewash are presented in graphical form for a number of values of θ_0, a Mach number—leading-edge-sweep parameter. Sidewash calculated from the lifting-line formula has been compared with the lifting-surface sidewash for values of θ_0 of 0.40 and 1.00. This comparison shows very good agreement of the lifting-line results with lifting-surface results except at the higher vertical distances close behind the trailing edge for $\theta_0=1.00$. The curves for $\theta_0=0.40$ reveal that, as θ_0 is decreased from 1.00, the agreement close behind the trailing edge improves.

An illustrative calculation of the sidewash-induced force on a half-delta vertical tail operating behind a triangular wing indicates that the induced force acts in opposition and is comparable in magnitude to the damping force created on the isolated rolling tail. In order to determine the total force which would act on the vertical tail of a steady-rolling aircraft in flight, an additional force induced by the aileron sidewash should be calculated. This force may be of the same order of magnitude as, and opposed to, the force induced on the tail by the wing sidewash. No attempt has been made in the present report to evaluate aileron sidewash.

LANGLEY AERONAUTICAL LABORATORY,
NATIONAL ADVISORY COMMITTEE FOR AERONAUTICS,
LANGLEY FIELD, VA., *October 21, 1955.*

APPENDIX A

TREATMENT OF SINGULARITIES IN $v_{P,E}$ AS GIVEN BY EQUATION (20)

In order to isolate the "infinite" terms, equation (23) may be written as

$$v_{P,E}=\frac{z H\beta^2}{\pi}\left[\int_0^f \frac{dx_1}{\theta_0 x_1}\,k_2(-2K_2+E_2)+\int_0^f \frac{dx_1}{\theta_0 x_1}\,k_2\frac{E_2}{1-k_2^2}+\int_f^c \frac{dx_1}{\theta_0 x_1}\frac{1}{k_1^2}(-K_1+E_1)-\int_f^c \frac{dx_1}{\theta_0 x_1}\frac{E_1}{1-k_1^2}\right] \tag{A1}$$

(① ② ③ ④)

Terms ① and ③ are integrable by numerical methods, whereas terms ② and ④ contain a first-order infinity at the limit $x_1=f$ (when $x_1=f$, $k_1=k_2=1$).

Consider term ② in equation (A1)

$$\int_0^f \frac{dx_1}{\theta_0 x_1}\frac{k_2 E_2}{1-k_2^2}$$

If k_2 is replaced by its equivalent (see symbols), term ② becomes

$$\int_0^f \frac{dx_1}{(x-x_1)^2-\beta^2z^2-\theta_0^2x_1^2}\,E_2\sqrt{(x-x_1)^2-\beta^2z^2} \tag{A2}$$

Assume expression (A2) to be of the form $\int_0^f u\,dv$, where

$$u=E_2\sqrt{(x-x_1)^2-\beta^2z^2}$$

and

$$dv=\frac{dx_1}{(x-x_1)^2-\beta^2z^2-\theta_0^2x_1^2}$$

Then,

$$v=\frac{1}{\sqrt{\theta_0^2x^2+\beta^2z^2(1-\theta_0^2)}}\coth^{-1}\frac{-(1-\theta_0^2)x_1+x}{\sqrt{\theta_0^2x^2+\beta^2z^2(1-\theta_0^2)}}$$

$$du=\frac{\theta_0(E_2-K_2)}{k_2}-\frac{K_2k_2(x-x_1)}{\theta_0x_1}$$

and a parts integration of expression (A2) gives

$$\frac{E_2\sqrt{(x-x_1)^2-\beta^2z^2}}{\sqrt{\theta_0^2x^2+\beta^2z^2(1-\theta_0^2)}}\coth^{-1}\frac{-(1-\theta_0^2)x_1+x}{\sqrt{\theta_0^2x^2+\beta^2z^2(1-\theta_0^2)}}\Bigg|_0^f-\int_0^f\frac{\coth^{-1}\dfrac{-(1-\theta_0^2)x_1+x}{\sqrt{\theta_0^2x^2+\beta^2z^2(1-\theta_0^2)}}}{\sqrt{\theta_0^2x^2+\beta^2z^2(1-\theta_0^2)}}\left[\frac{\theta_0(E_2-K_2)}{k_2}-\frac{K_2k_2(x-x_1)}{\theta_0x_1}\right]dx_1 \tag{A3}$$

Substituting for k_1 its equivalent in term ④ of equation (A1) results in

$$-\int_f^c\frac{\theta_0x_1E_1\,dx_1}{\theta_0^2x_1^2-(x-x_1)^2+\beta^2z^2} \tag{A4}$$

With

$$u=\theta_0x_1E_1$$

and

$$dv=\frac{-dx_1}{\theta_0^2x_1^2-(x-x_1)^2+\beta^2z^2}$$

a parts integration of expression (A4) yields

$$\frac{\theta_0x_1E_1}{\sqrt{\theta_0^2x^2+\beta^2z^2(1-\theta_0^2)}}\tanh^{-1}\frac{-(1-\theta_0^2)x_1+x}{\sqrt{\theta_0^2x^2+\beta^2z^2(1-\theta_0^2)}}\Bigg|_f^c-\int_f^c\tanh^{-1}\frac{-(1-\theta_0^2)x_1+x}{\sqrt{\theta_0^2x^2+\beta^2z^2(1-\theta_0^2)}}\left[K_1\theta_0-\frac{(E_1-K_1)(x-x_1)}{\theta_0x_1k_1^2}\right]dx_1 \tag{A5}$$

The nonintegral term in expression (A5) may be written in slightly different form as

$$\frac{E_1\sqrt{(x-x_1)^2-\beta^2z^2}}{k_1\sqrt{\theta_0^2x^2+\beta^2z^2(1-\theta_0^2)}}\tanh^{-1}\frac{-(1-\theta_0^2)x_1+x}{\sqrt{\theta_0^2x^2+\beta^2z^2(1-\theta_0^2)}}\Bigg|_f^c \tag{A6}$$

Inasmuch as when $x_1=f$, $k_1=k_2=1$, it is clear that the evaluation of the integrated term in expression (A5) (equivalent to expression (A6)) at the limit $x_1=f$ will cancel the integrated term of expression (A3) evaluated at this same limit. The complete expression for $v_{P,E}$ is now seen to be

$$v_{P,E}=\frac{zH\beta^2}{\pi}\left\{\int_0^f\frac{dx_1}{\theta_0x_1}k_2(-2K_2+E_2)+\int_f^c\frac{dx_1}{\theta_0x_1}\frac{-K_1+E_1}{k_1^2}-\int_0^f\frac{\coth^{-1}\left[\dfrac{-(1-\theta_0^2)x_1+x}{\sqrt{\theta_0^2x^2+\beta^2z^2(1-\theta_0^2)}}\right]}{\sqrt{\theta_0^2x^2+\beta^2z^2(1-\theta_0^2)}}\left[\frac{\theta_0(E_2-K_2)}{k_2}-\frac{k_2K_2(x-x_1)}{\theta_0x_1}\right]dx_1-\int_f^c\frac{\tanh^{-1}\left[\dfrac{-(1-\theta_0^2)x_1+x}{\sqrt{\theta_0^2x^2+\beta^2z^2(1-\theta_0^2)}}\right]}{\sqrt{\theta_0^2x^2+\beta^2z^2(1-\theta_0^2)}}\left[K_1\theta_0-\frac{(E_1-K_1)(x-x_1)}{\theta_0x_1k_1^2}\right]dx_1-\frac{\pi\sqrt{x^2-\beta^2z^2}}{2\sqrt{\theta_0^2x^2+\beta^2z^2(1-\theta_0^2)}}\coth^{-1}\frac{x}{\sqrt{\theta_0^2x^2+\beta^2z^2(1-\theta_0^2)}}+\frac{\theta_0cE_{1,0}}{\sqrt{\theta_0^2x^2+\beta^2z^2(1-\theta_0^2)}}\tanh^{-1}\frac{[-(1-\theta_0^2)c+x]}{\sqrt{\theta_0^2x^2+\beta^2z^2(1-\theta_0^2)}}\right\} \tag{A7}$$

This equation in nondimensional form is presented in the analysis of the report as equation (24).

APPENDIX B

EVALUATION OF $v_{W,D}$

The contribution of the doublets distributed in the wake to the sidewash in region D is given by equation (28) as

$$v_{W,D}=\frac{3H(x-c)\theta_0^3c^3k_{2,0}}{\pi\beta^2z^3}\int_0^1\frac{s^2\sqrt{1-s^2}\,ds}{\left(1+\frac{\theta_0^2c^2}{z^2\beta^2}s^2\right)^2\sqrt{1-k_{2,0}^2s^2}}-\frac{H(x-c)^3\theta_0ck_{2,0}^3}{\pi\beta^2z^3}\int_0^1\frac{s^2\sqrt{1-s^2}\,ds}{\left(1+\frac{\theta_0^2c^2}{z^2\beta^2}s^2\right)^2(1-k_{2,0}^2s^2)^{3/2}} \tag{B1}$$

which by use of partial fractions can also be written

$$v_{W,D}=\frac{3H(x-c)\beta a^3k_{2,0}}{\pi}\left[\frac{1}{a^2}\int_0^1\frac{\sqrt{1-s^2}\,ds}{(1+a^2s^2)\sqrt{1-k_{2,0}^2s^2}}-\frac{1}{a^2}\int_0^1\frac{\sqrt{1-s^2}\,ds}{(1+a^2s^2)^2\sqrt{1-k_{2,0}^2s^2}}\right]-$$

$$\frac{H(x-c)^3ak_{2,0}^3}{\pi\beta z^2}\left[\frac{a^2}{(a^2+k_{2,0}^2)^2}\int_0^1\frac{\sqrt{1-s^2}\,ds}{(1+a^2s^2)\sqrt{1-k_{2,0}^2s^2}}-\frac{1}{a^2+k_{2,0}^2}\int_0^1\frac{\sqrt{1-s^2}\,ds}{(1+a^2s^2)^2\sqrt{1-k_{2,0}^2s^2}}+\frac{k^2}{(a^2+k_{2,0}^2)^2}\int_0^1\frac{\sqrt{1-s^2}\,ds}{(1-k_{2,0}^2s^2)^{3/2}}\right] \tag{B2}$$

For ease in writing, $\frac{\theta_0c}{z\beta}$ has been replaced by a in equation (B2). Consider first the integral

$$\int_0^1\frac{\sqrt{1-s^2}\,ds}{(1+a^2s^2)\sqrt{1-k_{2,0}^2s^2}} \tag{B3}$$

If the variable transformation $s=\sin\theta$ is made, expression (B3) becomes

$$\int_0^{\pi/2}\frac{\cos^2\theta\,d\theta}{(1+a^2\sin^2\theta)\sqrt{1-k_{2,0}^2\sin^2\theta}} \tag{B4}$$

The evaluation of expression (B4) is given by formula (9), table 61 of reference 16 as

$$\int_0^1\frac{\sqrt{1-s^2}\,ds}{(1+a^2s^2)\sqrt{1-k_{2,0}^2s^2}}=\frac{\sqrt{a^2+1}}{a\sqrt{a^2+k_{2,0}^2}}G(k_{2,0},a) \tag{B5}$$

where

$$G(k_{2,0},a)=\left[\frac{\pi}{2}+(K_{2,0}-E_{2,0})F(\cot^{-1}a,k_{2,0}')-K_{2,0}E(\cot^{-1}a,k_{2,0}')\right] \tag{B6}$$

Expression (B4) could also have been integrated without recourse to tables with the aid of reference 17 (pp. 134 to 136). The integration of expression (B3)

$$\int_0^1\frac{\sqrt{1-s^2}\,ds}{(1+a^2s^2)^2\sqrt{1-k_{2,0}^2s^2}}$$

may be performed by using the relationship (see p. 13 of ref. 17 and p. 79 of ref. 18):

$$\int_0^1\frac{\sqrt{1-s^2}\,ds}{(1+a^2s^2)^2\sqrt{1-k_{2,0}^2s^2}}=\int\frac{\sqrt{1-s^2}\,ds}{(1+a^2s^2)\sqrt{1-k_{2,0}^2s^2}}+a^2\frac{d}{d(a^2)}\int\frac{\sqrt{1-s^2}\,ds}{(1+a^2s^2)\sqrt{1-k_{2,0}^2s^2}} \tag{B7}$$

From equations (B5) and (B6), equation (B7) becomes

$$\int_0^1\frac{\sqrt{1-s^2}\,ds}{(1+a^2s^2)^2\sqrt{1-k_{2,0}^2s^2}}=\frac{\sqrt{a^2+1}}{a\sqrt{a^2+k_{2,0}^2}}G(k_{2,0},a)+a^2\frac{d}{d(a^2)}\left[\frac{\sqrt{a^2+1}}{a\sqrt{a^2+k_{2,0}^2}}G(k_{2,0},a)\right] \tag{B8}$$

Carrying out the differentiation in equation (B8) results in

$$\int_0^1\frac{\sqrt{1-s^2}\,ds}{(1+a^2s^2)^2\sqrt{1-k_{2,0}^2s^2}}=\frac{\sqrt{a^2+1}}{a\sqrt{a^2+k_{2,0}^2}}G(k_{2,0},a)-\frac{1}{2}\left[\frac{a\sqrt{a^2+1}}{(a^2+k_{2,0}^2)^{3/2}}+\frac{1}{a\sqrt{(a^2+1)(a^2+k_{2,0}^2)}}\right]G(k_{2,0},a)+$$

$$\frac{1}{2}\frac{\sqrt{a^2+1}}{\sqrt{a^2+k_{2,0}^2}}\left[K_{2,0}\sqrt{\frac{a^2+k_{2,0}^2}{(a^2+1)^3}}-\frac{K_{2,0}-E_{2,0}}{\sqrt{(a^2+1)(a^2+k_{2,0}^2)}}\right] \tag{B9}$$

The remaining integration needed to evaluate $v_{W,D}$ (eq. (B2)) is

$$\int_0^1 \frac{\sqrt{1-s^2}\,ds}{(1-k_{2,0}{}^2s^2)^{3/2}}$$

This integration may be reduced to standard elliptic forms by the transformation $s=\text{sn}\ u$ and integrated to give

$$\int_0^1 \frac{\sqrt{1-s^2}\,ds}{(1-k_{2,0}{}^2s^2)^{3/2}}=\frac{K_{2,0}-E_{2,0}}{k_{2,0}{}^2} \tag{B10}$$

The sidewash $v_{W,D}$ is now completely defined by equations (B2), (B5), (B9), and (B10) as

$$v_{W,D}=\frac{3H(x-c)\beta k_{2,0}a}{2\pi}\left\{\left[\frac{a\sqrt{a^2+1}}{(a^2+k_{2,0}{}^2)^{3/2}}+\frac{1}{a\sqrt{a^2+1}\sqrt{a^2+k_{2,0}{}^2}}\right]G(k_{2,0},a)-\frac{\sqrt{a^2+1}}{\sqrt{a^2+k_{2,0}{}^2}}\left[K_{2,0}\frac{\sqrt{a^2+k_{2,0}{}^2}}{(a^2+1)^{3/2}}-\frac{K_{2,0}-E_{2,0}}{\sqrt{a^2+1}\sqrt{a^2+k_{2,0}{}^2}}\right]\right\}-$$

$$\frac{H(x-c)^3ak_{2,0}{}^3}{\pi\beta z^2}\left\{\left[\frac{-\sqrt{a^2+1}}{a(a^2+k_{2,0}{}^2)^{3/2}}+\frac{3a\sqrt{a^2+1}}{2(a^2+k_{2,0}{}^2)^{5/2}}+\frac{1}{2a\sqrt{a^2+1}\,(a^2+k_{2,0}{}^2)^{3/2}}\right]G(k_{2,0},a)-\frac{K_{2,0}}{2(a^2+1)(a^2+k_{2,0}{}^2)}-\frac{3(E_{2,0}-K_{2,0})}{2(a^2+k_{2,0}{}^2)^2}\right\} \tag{B11}$$

Considerable simplification of equation (B11) may be accomplished by combining terms and noting that

$$a^2+k_{2,0}{}^2=\frac{(x-c)^2k_{2,0}{}^2}{\beta^2z^2}=\frac{(x-c)^2k_{2,0}{}^2a^2}{\theta_0{}^2c^2}$$

and

$$v_{W,D}=\frac{H\beta\theta_0c}{\pi}\left[\frac{2+a^2}{a\sqrt{a^2+1}}G(k_{2,0},a)-\frac{a(x-c)k_{2,0}}{\theta_0c(a^2+1)}K_{2,0}\right] \tag{B12}$$

Replacing a by its nondimensional equivalent

$$a=\frac{\theta_0c}{\beta z}=\frac{1}{z_0}$$

and H by its equivalent and then nondimensionalizing x by c and $v_{W,D}$ by $pb/2$ gives

$$\frac{v_{W,D}}{pb/2}=\frac{2}{\pi G(\theta_0)}\left[\frac{2z_0{}^2+1}{\sqrt{z_0{}^2+1}}G\left(k_{2,0},\frac{1}{z_0}\right)-\frac{K_{2,0}k_{2,0}(x_0-1)z_0}{\theta_0(z_0{}^2+1)}\right] \tag{B13}$$

Equation (B13) is identical with equation (29) of the analysis, with the exception that, in the analysis, the function $G\left(k_{2,0},\frac{1}{z_0}\right)$ has been written out.

REFERENCES

1. Lomax, Harvard, Sluder, Loma, and Heaslet, Max. A.: The Calculation of Downwash Behind Supersonic Wings With an Application to Triangular Plan Forms. NACA Rep. 957, 1950.
2. Martin, John C.: The Calculation of Downwash Behind Wings of Arbitrary Plan Form at Supersonic Speeds. NACA TN 2135, 1950.
3. Harmon, Sidney M., and Jeffreys, Isabella: Theoretical Lift and Damping in Roll of Thin Wings With Arbitrary Sweep and Taper at Supersonic Speeds—Supersonic Leading and Trailing Edges. NACA TN 2114, 1950.
4. Brown, Clinton E., and Adams, Mac C.: Damping in Pitch and Roll of Triangular Wings at Supersonic Speeds. NACA Rep. 892, 1948. (Supersedes NACA TN 1566.)
5. Jahnke, Eugene, and Emde, Fritz: Tables of Functions. Fourth ed., Dover Publications, 1945.
6. Whittaker, E. T., and Watson, G. N.: A Course of Modern Analysis. American ed., The Macmillan Co., 1948, ch. 22.
7. Kahane, A.: Theory of Subsonic and Supersonic Sidewash Induced by a Wing in Roll. Rep. No. EDR–57–154, Republic Aviation Corp., May 20, 1953.
8. Mirels, Harold, and Haefeli, Rudolph C.: Line-Vortex Theory for Calculation of Supersonic Downwash. NACA Rep. 983, 1950.
9. Robinson, A.: On Source and Vortex Distributions in the Linearised Theory of Steady Supersonic Flow. Rep. No. 9, College of Aero., Cranfield (British), Oct. 1947.
10. Schlichting, H.: Tragflügeltheorie bei Überschallgeschwindigkeit Luftfahrtforschung, Bd. 13, Nr. 10, Oct. 12, 1936, pp. 313–335.
11. Martin, John C., Diederich, Margaret S., and Bobbitt, Percy J.: A Theoretical Investigation of the Aerodynamics of Wing-Tail Combinations Performing Time-Dependent Motions at Supersonic Speeds. NACA TN 3072, 1954.
12. Margolis, Kenneth, and Bobbitt, Percy J.: Theoretical Calculations of the Pressures, Forces, and Moments at Supersonic Speeds Due to Various Lateral Motions Acting on Thin Isolated Vertical Tails. NACA Rep. 1268, 1956. (Supersedes NACA TN 3373 by Margolis and TN 3240 by Bobbitt.)
13. Michael, William H., Jr.: Analysis of the Effects of Wing Interference on the Tail Contributions to the Rolling Derivatives. NACA Rep. 1086, 1952. (Supersedes NACA TN 2332.)
14. Silverstein, Abe, Katzoff, S., and Bullivant, W. Kenneth: Downwash and Wake Behind Plain and Flapped Airfoils. NACA Rep. 651, 1939.
15. Spreiter, John R., and Sacks, Alvin H.: The Rolling Up of the Trailing Vortex Sheet and Its Effect on the Downwash Behind Wings. Jour. Aero. Sci., vol. 18, no. 1, Jan. 1951, pp. 21–32, 72.
16. De Haan, D. Bierens: Nouvelles Tables D'Intégrales Définies. G. E. Stechert & Co. (New York), 1939, p. 96.
17. Cayley, Arthur: An Elementary Treatise on Elliptic Functions. Second ed., George Bell and Sons (London), 1895.
18. Roberts, W. R. Westropp: Elliptic and Hyperelliptic Integrals and Allied Theory. Cambridge Univ. Press, 1938.